ABSTRACT

MEYER, ARIC P. Optical and Electrical Enhancement of Organic Solar Cells. (Under the direction of Harald Ade).

Organic solar cells have the potential to offer low cost, mass produced, solar energy generation, but further research is required to increase efficiency, improve lifetime, and reduce production costs before the low cost goal can be achieved. Current research toward improving efficiency is focused on developing new materials with better absorption and charge transport properties, and on improving morphology. There are other pursuits that could also significantly improve efficiency yet are relatively neglected by researchers. Two of these are optical light trapping to increase absorption and control of interfaces to reduce energy loss. This thesis makes contributions to both of these goals in three ways. First, some surprising results from the optical modeling of organic solar cells at non-normal incidence are described. Second, a general method for assessing the potential of a promising light trapping geometry is introduced, and discrepancies between modeling and experiment of that structure are explained. Finally, the effect of air exposure on single material and bulk heterojunction solar cells with InGa cathode is investigated. Air exposure is found to increase open circuit voltage, and using this method the open circuit voltage of a common organic solar cell system is increased by 15%. This work exposes the current lack of knowledge of many aspects of band structure in organic solar cells which suggests the need for more research in this area.

Optical and Electrical Enhancement of Organic Solar Cells

by
Aric Paul Meyer

A thesis submitted to the Graduate Faculty o
North Carolina State University
in partial fulfillment of the
requirements for the Degree of
Master of Science

Physics

Raleigh, North Carolina

2009

APPROVED BY:

_____	_____
Jack Rowe	Keith Weninger

_____
Harald Ade
Chair of Advisory Comittee

BIOGRAPHY

Aric Meyer was born in Grand Rapids, MI and received a B.S. in physics from Grand Valley State University in Allendale, MI in 2000. He entered graduate school at North Carolina State University in January, 2007. In the intervening years, Aric taught English in China, ran a small import business, taught university physics, got married, and had two children (a third was born during graduate school). He now works for CEI, makers of EnSight software, in Apex, NC.

TABLE OF CONTENTS

LIST OF TABLES

LIST OF FIGURES

CHAPTER 1

Introduction

1.1 Motivation

Solar energy is abundant and underused. The same amount of energy used in the world in 2006[1] strikes the earth's surface in the form of sunlight every 90 minutes, yet solar energy accounted for only 0.54% of human energy use in 2007[2] (not including passive solar heating and the heat and light used by biological systems). The contrast between these two statistics is striking, and reflects solar's high cost, difficulty with large scale production, and reliance on newer technology compared with fossil fuels. In order for solar to replace fossil fuels the problems of cost and mass production must be solved.

Photovoltaics are devices which convert light directly into electricity. Figure 1.1 gives the history of power conversion efficiencies for various photovoltaic technologies. Inorganic solar cells have power conversion efficiencies and lifetimes several times higher than organics. More importantly organics are not ever expected to match inorganics in either benchmark. However, organic solar cells hold the promise of cheap mass production, with the potential to be the cheapest form of solar energy measured in $/W.

The field of organic solar cells is young, exciting, and full of promise. In a Department of Energy report on solar energy utilization[3], organic materials were a critical part of many of 'priority research directions.' Searching Web of Science reveals the rapid rise the organic photovoltaic field has undergone in recent years (Figure 1.2).

1.2 Solar cell basics

A solar cell is a photodiode which can be modeled using a simple 'equivalent circuit.' Doing so allows for powerful and convenient characterization of devices. An ideal diode has an exponential I-V relationship, and does not allow any current to flow in one direction. A real

diode will always have some limit to how low the resistance can go and will allow some leakage current. Therefore a real photodiode is often represented by a circuit consisting of an ideal photodiode and two resistors (Figure 1.3). The series resistor (R_s) limits the current at high external voltages and the parallel or shunt resistor (R_p) allows some current to flow in the reverse direction (leakage current).

The effects of each circuit element can be seen by viewing a semilog plot of a photodiodes' I-V curve (Figure 1.4). Two curves are shown. The dark current is when the photodiode is in the dark (identical to an ordinary diode); under illumination the diode circuit element produces a photocurrent. At low voltages, the diode resistance is high, so a small amount a current flows through the parallel resistor (marked "parallel resistance"). As the external voltage increases the diode resistance drops and the current increases exponentially. At high enough voltage the resistance of the diode becomes close to that of the series resisitor, and the I-V relationship becomes linear. In designing solar cells it is usually desired to make cells which are most like ideal diodes by minimizing the series resistance and maximizing the shunt, i.e. parallel, resistance. When analyzing power output the I-V curve is usually viewed on a linear scale over a smaller voltage range like in Figure 1.5. In the fourth quadrant, when current opposes the external voltage, the solar cell produces power. The power output of a solar cell is equal to the product of its current and voltage under operating conditions. In basic solar cell research it is assumed that the cell can be operated at its maximum power point, which is the point on the I-V curve where $I \times V$ reaches its maximum. A few other quantities are helpful in characterizing a solar cell, those being the open-circuit voltage (V_{OC}), short-circuit current (I_{SC}), and fill factor (FF). The V_{OC} is mostly determined by the electronic structure of the device. I_{SC} is a measure of absorption and internal quantum efficiency (IQE), and FF is related to the quality of the diode. Since $PCE = V_{OC} \times I_{SC} \times FF$, increasing any one factor without reducing the others will increase the overall efficiency of the device.

1.3 Organic electronics

The basis of organic conductors and semiconductors is delocalized π electrons. In covalent bonding, bonding electrons are typically shared between only 2 atoms. However,

carbon can form rings and chains of conjugated bonds. Conjugated bonds can be expressed as alternating single and double bonds, but in reality the π orbitals extend along both bonds and overlap with the orbitals of other atoms. They form a single molecular orbital in which electrons are delocalized over many carbon atoms, allowing charges to flow freely within the orbital. π orbitals from adjacent molecules (or sections of a polymer chain) can also overlap, which further delocalizes electrons.

Since organic semiconductors are molecular and not, in general, crystallized, chemistry terminology is most often used to describe their electronic properties. Many of the terms used have counterparts in semiconductor physics. Table 1.1 gives some common terms and their solid state analogs.

As with inorganic semiconductors, organic semiconductors have an energy gap between their HOMO and LUMO levels. Since organics lack the rigid crystal structure of inorganics, doping is done chemically by adding elements with differing electronegativity rather than materials with different numbers of valence electrons. The resulting charge transfer creates holes in the HOMO and/or electrons the LUMO. In general it is difficult to control the properties of organics through doping, so most organic materials are used either as intrinsic semiconductors or as conductors.

Organic and inorganic semiconductors differ in a way that fundamentally affects the functioning of photovoltaic cells. When inorganics (for example, a Si p-n junction cell) absorb a photon, an electron is energized into the conduction band, leaving a hole in the valence band. The other electrons in the material screen the electron and hole from each other, reducing their binding energy to below kT. The electron and hold can then move independently, making them free charge carriers which can travel to their respective electrodes.

Organic materials on the other hand do not screen charges as well. The electron and hole still ‘attract’ each other and form a quasi-particle called an exciton. These excitons typically have a binding energy of ~0.2eV, which is much larger than kT (~0.025eV), and therefore cannot spontaneously dissociate; however, it can move about by diffusion as a neutral quasi-particle.

In order to overcome the binding energy and split an exciton, two materials with different energy levels are put in contact. This results in an electric field at the interface. When an exciton reaches the vicinity of such an interface the electric field (if strong enough) pulls apart the exciton. The electron ends up in the LUMO of the electron-acceptor material and the hole in the HOMO of the electron-donor. Except in cases where the charges are still bound across the interface (called an exciplex), the electron and hole are now free charge carriers and can travel to the electrodes for collection.

This mechanism is fundamental to the device physics of 'excitonic photovoltaic cells' and is responsible for confusion in the early OPV literature, especially with regard to the origin of the open-circuit voltage. As explained in Ref. 4, in inorganic photovoltaics the chemical potentials of the electrons and holes are identical to each other since they are formed at the same locations. A built in potential must be applied (via the work function difference of the electrodes) to force the charges in opposite directions. In an excitonic cell the free charge carriers are formed on opposite sides of an interface. Both the chemical potential and the space-charge drive charges toward the electrodes.

The need to split excitons dominates organic solar cell design. Excitons are short-lived, with diffusion lengths often less than 10 nm. Exciton diffusion lengths approaching 100 nm are very rare. Bilayer solar cells which split excitons at the interface between the two materials are severely limited in thickness. To overcome this limitation, the bulk heterojunction was created. An ideal bulk heterojunction (BHJ) is a bicontinuous network of two materials where each phase is much smaller than the exciton diffusion length. With the exciton-splitting interface spread throughout the bulk most excitons can be split; continuous paths in each material back to the electrodes allows charges to be collected.

The BHJ structure is far superior to the bilayer, but is still quite limited. Organic semiconductors have lower charge mobility than inorganics. The need to mix two or more materials in a BHJ further limits charge transport and therefore layer thickness, leading to a trade-off between thicker layers for increased absorption and thinner layers for improved collection efficiency. Thicker active layers will absorb more light and generate more excitons,

however the excitons must be separated and free charge carriers pairs must be collected at the electrodes in order to generate a photocurrent. Thick layers force charges to recombine before reaching the electrodes leading to lower photocurrent. Thicker layers can also increase a domain size, which lowers exciton dissociation rates. This leads to optimized devices having active layers from <50 nm to a few hundred nanometers depending on the materials. At these thicknesses a significant portion of incident light is not absorbed.

1.4 Optics in organic solar cells

While most researchers focus on developing new materials, new material combinations, and controlling morphology to increase absorption and improve electrical properties, other methods to work with current limitations have been investigated. One of those is by changing the geometry of the solar cells. Several alternative geometries to the standard planar geometry have been tested with promising results. While solar cell geometry in inorganic cells usually involves concentrating light onto a small area, in organic cells the purpose is to increase absorption and/or allow for thinner layers. Organic layers are so thin that interference, especially from the reflection off the back electrode, can strongly affect total absorption.

Perhaps the simplest optical variation is to use two transparent electrodes so there is no strong reflection. Besides the material limitations inherent in this method, reducing the reflection eliminates the potential to benefit from the interference. Nearly as simple is to keep the reflective cathode and add a transparent 'spacer layer' between the active layer(s) and reflective cathode to control the position of the interference pattern relative to the active layer.[5] As shown in Ref. 6, this method can only benefit cells with extremely thin (>~60 nm) active layers. Methods to scatter incoming light at the surface or upon reflection have also been proposed. Polymer solar cells have even been fabricated around the core of an optical fiber.[7] Light incident on the end of the fiber becomes trapped inside, increasing absorption. The new structure promises high efficiency, but would likely be difficult to manufacture.

A simple light trapping scheme based on a 'V'-shaped solar has been demonstrated.[8] This structure holds the promise of both improved efficiency and ease of manufacturing, but still requires optimization. The structure will be analyzed in chapter 3.

1.5 Introduction to the remaining chapters

The body of this thesis consists of three self-contained articles to be submitted for publication.

Chapter 2 details the changes to the optical electric field distribution, and therefore absorption, vs. depth within an organic solar cell as the angle of incidence increases. Given the interdisciplinary nature of organic electronics a basic optical study could benefit researchers without an understanding of optics. Additionally, this work was motivated by several published misconceptions about the electric field at oblique angles, as noted in Chapter 2. Also, modeling non-normal incidence is required for non-planar geometries such as in chapter 3. This chapter is presented here as it was submitted to the Journal of Applied Physics on 5/24/2009.

Chapter 3 applies optical modeling to the 'V'-shaped or 'folded' architecture to introduce a general method for estimating the potential of the folded structure. The folded structure seems to hold much promise for overcoming the thickness limitations of organic solar cells, but so far publications on the folded structure have been 'proof of concept' type of work. We found that predictions from our model often do not agree with experiment, which is surprising considering the success of optical model of planar organic solar cells. Possible reasons for the discrepancy between experiment and model are explored in Chapter 3. One likely cause is the effects of substrate thickness which have not been considered previously. This chapter is currently in a late draft stage with the intent to publish in the Journal of Applied Physics.

Chapter 4 presents the fabrication of P3HT:PCBM solar cells with the highest-ever reported open circuit voltages. There are still many unknowns as to the maximum achievable V_{OC} and the loss mechanisms involved. Very few improvements to V_{OC} have been achieved in recent years. It is hoped that this paper will motivate further research into understanding and

controlling the interfaces in organic solar cells. Chapter 4 is in late draft stage for submission to Applied Physics Letters.

Table 1.1 Common organic semiconductor terms and their solid state analogs

Organic semiconductors	Semiconductor physics
Highest occupied molecular orbital (HOMO)	Valence band
Lowest unoccupied molecular orbital (LUMO)	Conduction band
Hole transport layer (HTL)	p-type material
Electron transport layer (ETL)	n-type material
Electron donor/acceptor	p/n-type material

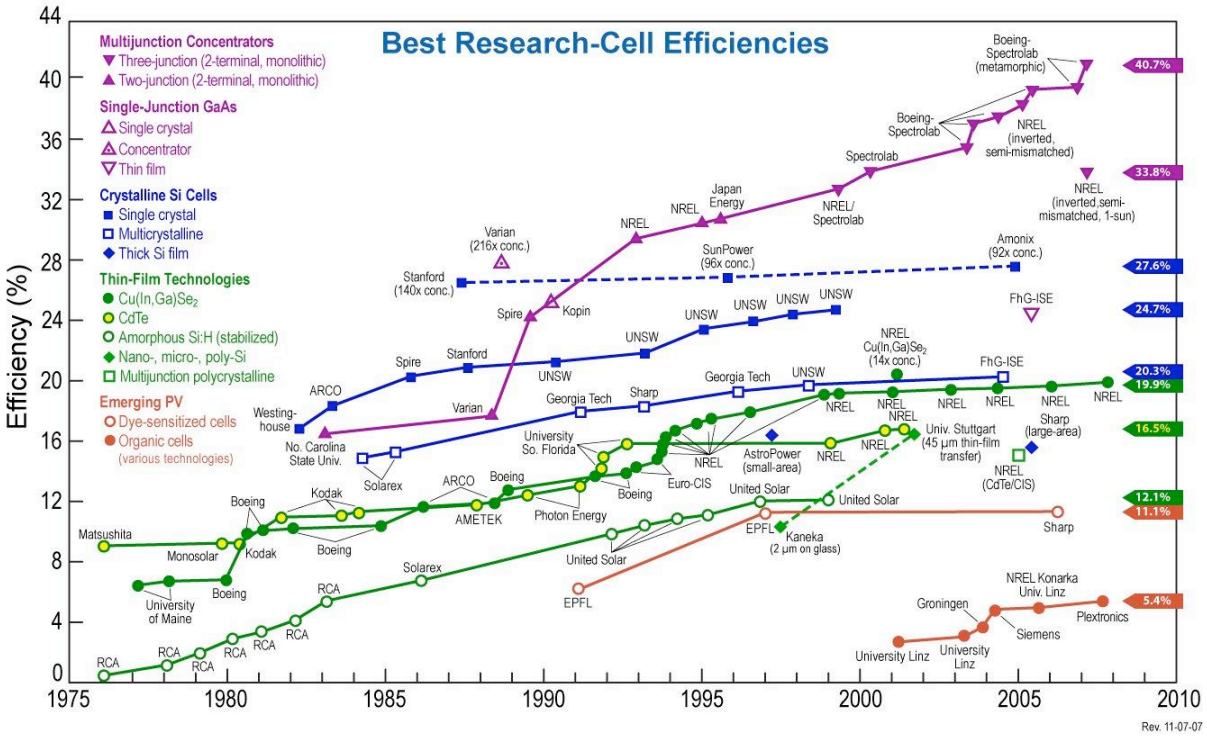

Figure 1.1. Historical chart of record efficiencies (certified) for different classes of solar cells.

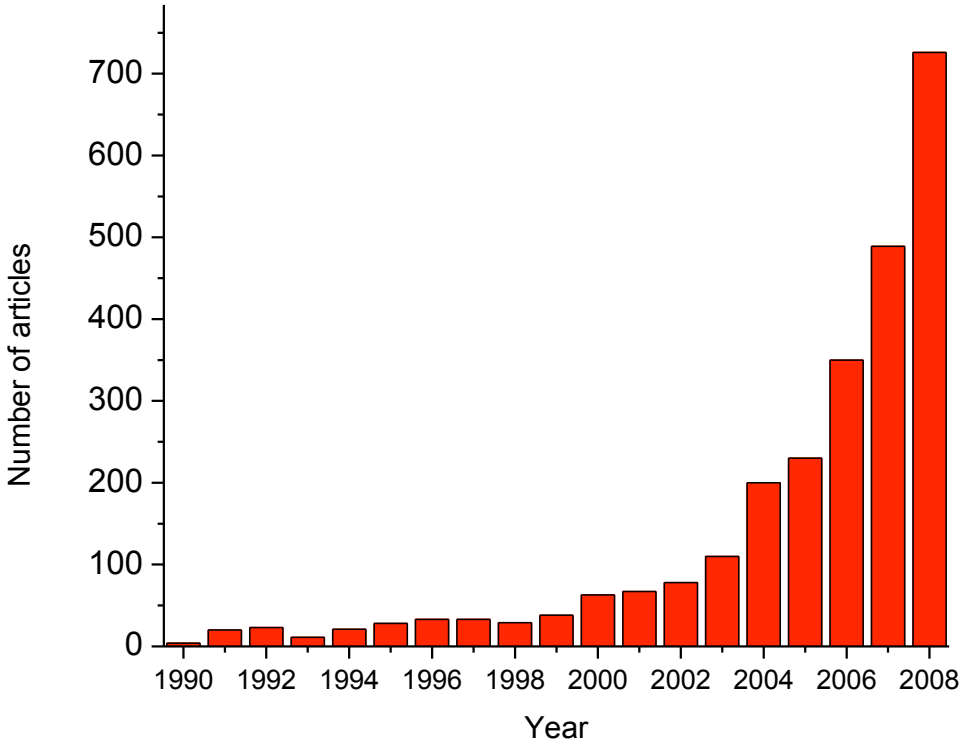

Figure 1.2. Number of hits found by searching Web of Science for the words: “organic” “solar” and “cells”, sorted by year of publication. Searched on 5/22/2009.

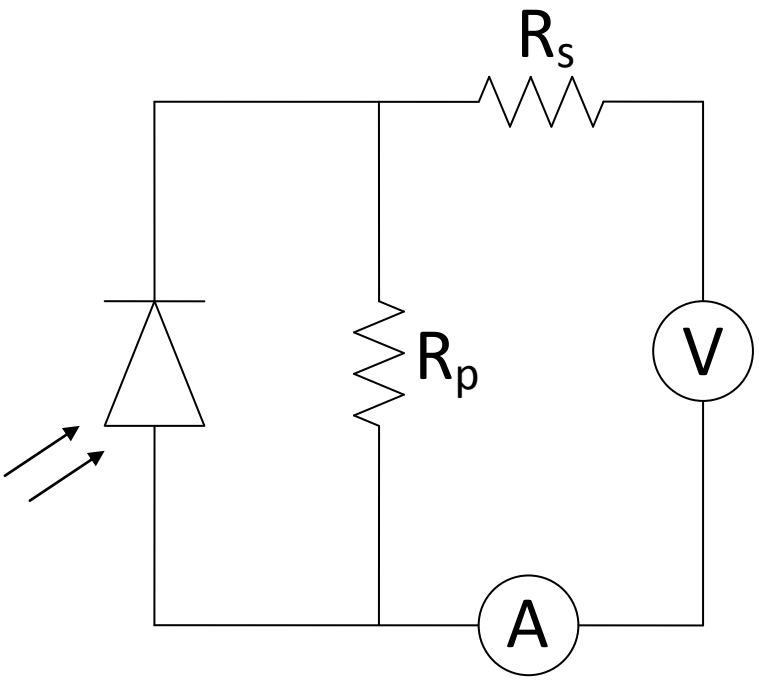

Figure 1.3. Equivalent circuit of a solar cell

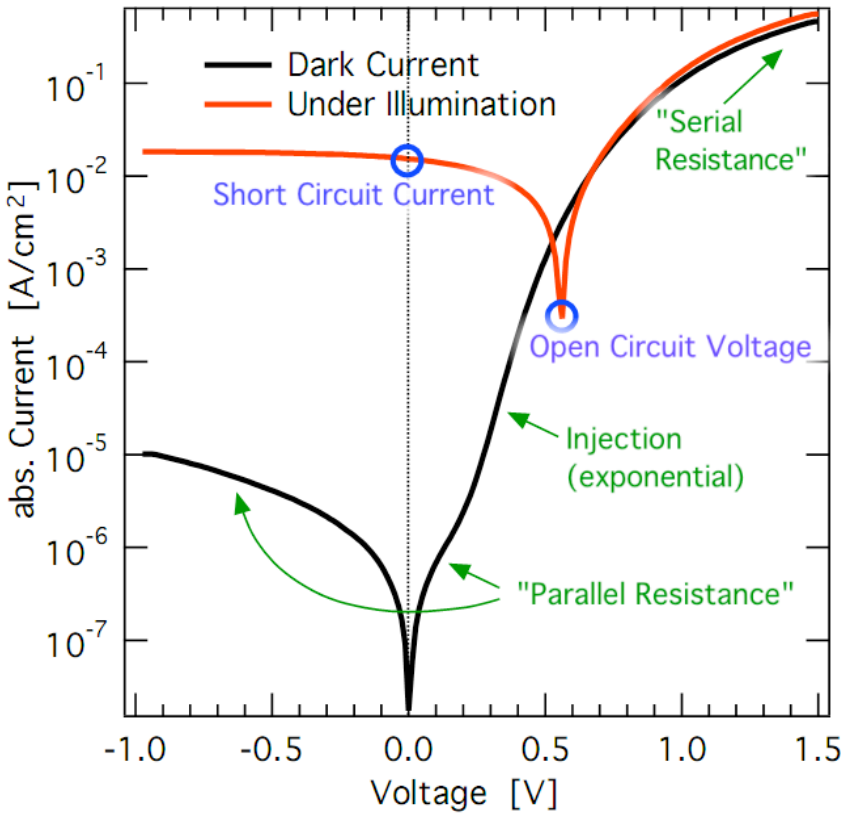

Figure 1.4. Typical solar cell I-V curve – log plot.

Image from Ref. 9

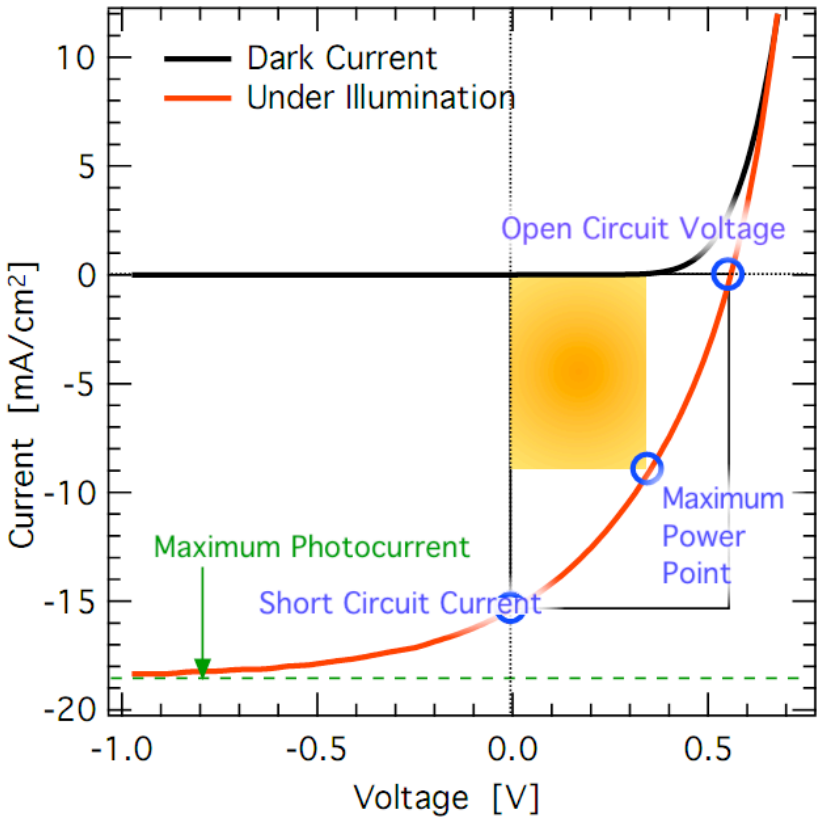

Figure 1.5. Typical solar cell I-V curve – linear plot.

Image from Ref. 9

References

[1] in *International Energy Annual 2006* (Energy Information Administration, 2008).

[2] BP 2007 Review of World Energy.

[3] Nathan S Lewis and George Crabtree, edited by Office of Basic Energy Science US Department of Energy (2005).

[4] Brian A. Gregg and Mark C. Hanna, "Comparing organic to inorganic photovoltaic cells: Theory, experiment, and simulation," J. Appl. Phys. 93 (6), 3605-3614 (2003).

[5] S. H. Kim J. Y. Kim, H.-H. Lee, K. Lee, W. Ma, X. Gong, A. J. Heeger,, "New Architecture for High-Efficiency Polymer Photovoltaic Cells Using Solution-Based Titanium Oxide as an Optical Spacer," Advanced Materials 18 (5), 572-576 (2006).

[6] B. Viktor Andersson, David M. Huang, Adam J. Moule et al., "An optical spacer is no panacea for light collection in organic solar cells," Applied Physics Letters 94 (4), 043302-043303 (2009).

[7] Jiwen Liu, Manoj A. G. Namboothiry, and David L. Carroll, "Fiber-based architectures for organic photovoltaics," Applied Physics Letters 90 (6), 063501-063503 (2007).

[8] M. Niggemann, M. Glatthaar, P. Lewer et al., "Functional microprism substrate for organic solar cells," Thin Solid Films 511-512, 628-633 (2006); Seung-Bum Rim, Shanbin Zhao, Shawn R. Scully et al., "An effective light trapping configuration for thin-film solar cells," Applied Physics Letters 91 (24), 243501-243503 (2007); Yinhua Zhou, Fengling Zhang, Kristofer Tvingstedt et al., "Multifolded polymer solar cells on flexible substrates," Applied Physics Letters 93 (3), 033302-033303 (2008).

[9] Carston Deibel, in *Notes on Disordered Matter* (2008).

CHAPTER 2

The effect of angle of incidence on the electric field distribution within thin film organic solar cells

A. Meyer and H. Ade

Department of Physics, North Carolina State University, Raleigh, NC 27695

The optical field within an organic solar cell is the result of thin film interference effects which become more complex at higher angles of incidence. We use optical modeling to study the electric field at oblique incidence. Our findings include an expansion of the interference pattern, a significant intensity of p-polarized light at the cathode interface, and a strong dependence on indium tin oxide (ITO) and poly(3,4-ethylenedioxythiophene) poly(styrenesulfonate) (PEDOT:PSS) thicknesses for single wavelengths. Applications to current research are presented including recent misconceptions in the literature and suggestions for novel research.

I. INTRODUCTION

Optical thin film interference strongly affects the efficiency of organic solar cells. In order to engineer optimal devices and control their complex interplay between optical, structural and electronic properties, the interference effects need to be thoroughly understood. Fortunately the interference can be modeled with simple and accurate methods, yielding reliable information about the total absorption and exciton distribution within a solar cell. Such simulations have proved invaluable to the study of organic solar cells and are now becoming a standard tool of solar cell analysis. Simulations have been used to determine optimum cell structure,[1] determine internal quantum efficiencies (IQE),[2,3] study charge carrier recombination,[4] and investigate novel geometries.[5]

Device testing and simulation are usually performed at normal incidence; however, two recent independent studies were performed to extend the use of optical modeling to non-normal incidence.[2,6] Both studies found that unlike inorganic solar cells, organic photovoltaics can benefit from oblique incidence. Though both studies correctly mentioned that the interference pattern within a cell changes with angle of incidence, their attempts to qualify the change were incomplete and sometimes inaccurate. One paper contains a graph of the electric field which is incorrect,[2,6] the other makes mistaken assumptions about the electric field distribution because the distribution was not explicitly calculated.[2]

Given the prevalence of optical simulations in solar cell research and specifically the use of electric field distribution in investigations of device physics it is important to have a correct understanding of electric fields inside organic solar cells. A better understanding of non-normal incidence would also benefit research toward promising new device geometries such as the 'folded' cell architecture.[5,7,8]

In this paper, we present a detailed analysis of the electric field within a solar cell at non-normal incidence. We use physical principles to discuss the changes that occur to the electric field distribution and present data from simulations to illuminate the discussion. It is found that the electric field distribution changes significantly due to a combination of many factors. We

apply our results to a discussion of IQE from recent literature and to an experiment of electrical losses at PEDOT:PSS and cathode interfaces.

II. THEORETICAL AND EXPERIMENTAL METHODS

This paper uses a Transfer Matrix Method (TMM) similar to the ones described in Refs. 2,9. The TMM is a well-established method for the optical modeling of stacks of thin layers and has been used extensively in organic solar cell literature. Though not in matrix form, the mathematics of TTM as used here are also described in Ref. 10.

When a plane wave strikes an interface between absorbing media (complex index of refraction) at non-normal incidence the refraction follows Snell's Law: $\tilde{n}_1 \sin\theta_1 = \tilde{n}_2 \sin\theta_2$ with complex $\tilde{n}$ and θ. When θ is complex it "no longer has the simple significance of an angle of refraction";[11] plane waves with complex θ are called inhomogeneous plane waves. For a discussion see, for example, the chapter 'Optics of Metals' in Ref. 11. For the purposes of this paper the plane waves can be treated conceptually as ordinary (homogeneous) plane waves with real θ, with calculations performed using complex θ. Another difference from TMM at normal incidence is that to calculate the total electric field for p-polarized light the fields of the two traveling waves (incident and reflected) must be added as vectors. The results have important implication for the continuity or discontinuity of the electric field at an interface.

Optical constants for glass, indium tin oxide (ITO), poly(3,4-ethylenedioxythiophene) poly(styrenesulfonate) (PEDOT:PSS), and poly(3-hexylthiophene):phenyl-C61-butyric acid methyl ester (P3HT:PCBM) were determined by fits to transmission measurements. ITO (ShinAn SNP) was used, and was etched clean for transmission measurements on glass. Films of PEDOT:PSS (Baytron P) and P3HT:PCBM (Sigma Aldrich : Nano-C) were spun cast on microscope glass slides at different spin rates to achieve films with different thicknesses. P3HT:PCBM films were annealed for 10 minutes at 110°C. Transmission data was acquired at normal and 60° incidence using a Cary 50SE spectrophotometer.

Optical modeling (TMM) of single layers and complete solar cells was performed using Mathematica and optical constants from the literature.[2,12] Results of the single layers were compared to the transmission data. Literature values of the optical constants for PEDOT:PSS gave good fits to the optical transmission measurement, so the literature values were used for PEDOT:PSS. Though optical anisotropy has been observed in spun cast films of PEDOT:PSS,[13] we believe the anisotropy is small enough to disregard for the wavelengths of interest. The anisotropy may need to be considered for solar cells that absorb longer wavelengths. For glass, ITO, and P3HT:PCBM the constants were fit to our transmission data but did not vary significantly from the original constants in 2. Constants for aluminum were taken from Ref. 12.

III. RESULTS

A plot of the normalized square of the electric field amplitude, $\left|\vec{E}\right|^2$, from simulation is displayed in Figure 2.2 at normal and 60° incidence for 500 nm light inside a solar cell with the following structure: glass / ITO (150nm) / PEDOT:PSS (50nm) / P3HT:PCBM (100nm) / Al (100nm). Several characteristic features are apparent. The interference pattern for 60° incident light is stretched compared to 0° incident light, shifting the peaks and valleys away from the metal cathode (Ref. 6 shows them moving toward the cathode). Also, the electric field for p-polarized light is discontinuous at the boundaries and does not drop to ~0 at the Al interface. In Ref. 6 the electric field, which presumably is unpolarized (contains 50/50 s/p-polarized light), is continuous at all interfaces. The peaks for s and p-polarized light in the ITO layer do not coincide; this is primarily because they undergo different phase shifts upon reflection at the PEDOT:PSS/P3HT:PCBM interface. A discussion of these characteristic effects and other related implications of interference in organic thin film devices follows below.

Expanding interference pattern

Every reflection at an interface within a solar cell contributes to the overall interference pattern of the electromagnetic wave but the effect is usually dominated by the strongly-reflecting metal cathode. Reflection of a traveling plane wave at a "hard" boundary such as a metal causes a phase shift of ~180° in the reflected wave. The actual phase shift and the depth the electric field can penetrate the electrode depends on the optical properties of the metal and is wavelength dependent. We have chosen Al as cathode material due to it prevalence in many experimental studies. Al has relatively constant properties over the wavelength range of interest here, which allows the discussion to focus on the implications of layer spacings and oblique illumination. The ~180° phase shift of the hard boundary reflection results in destructive interference near the cathode (a node), where the total electric field drops to nearly zero, and constructive interference at $\sim \lambda/4$ from the metal interface (the first antinode) where the field reaches a maximum. This effect is well known and is the main reason why optical modeling of thin film devices is necessary and successful in explaining a number of observations and device characteristics such as the drop in efficiency for active layer thicknesses over ~100nm. This drop is due to the light reflected from the cathode interfering with the incoming light in such a way that much of the incoming light is reflected at the PEDOT:PSS/P3HT:PCBM interface.

The familiar pattern of constructive and destructive interference is qualitatively preserved at oblique angles, but with increasing angle of incidence the distance between interference nodes and antinodes increases with $1/\cos\theta$, where θ is the angle of refraction (see Figure 2.1). Though one might expect the interference pattern to compress at higher angles since a wave travels farther within each layer and therefore has a large temporal phase shift, the interfere is actually produced by waves that are phase shifted in space relative to each other. The combined effects of the temporal and spatial phase shifts is to 'stretch out' the interference pattern normal to the interface; this result is consistent with Bragg's Law: $n\lambda = 2d\sin\phi$, where ϕ is the angle of incidence to the surface. In our notation, where θ denotes the angle to the interface normal, Bragg's Law would be written as $n\lambda = 2d\cos\theta$. As θ increases (and $\cos\theta$ decreases), d would

have to increase by $1/\cos\theta$ to maintain the interference condition, showing that distance between interference peaks increases with angle of incidence. Picturing interfering wave fronts due to reflection off an interface may help to visualize this phenomenon.

Though reflection from the cathode is most significant, interference in the other layers can also cause dramatic changes in efficiency. If the conditions for destructive and constructive interference are met, a thin film or stack of thin films acts to minimize or maximize reflection, respectively (e.g. anti-reflection coatings). These effects can be large, and are highly sensitive to film thickness, wavelength, and angle of incidence. One way to observe the effect through simulation is by comparing the absorption vs. layer thicknesses for solar cells at oblique and normal incidence. Figure 2.3 shows results for a Glass / ITO (150 nm) / PEDOT:PSS / P3HT:PCBM (100nm) / Al (100 nm) solar cell under 400 nm, 700 nm, and AM1.5G light illumination. For 400nm light, the cell can be from ~30% less efficient to 80% more efficient at 60° incidence relative to its efficiency at 0° incidence, depending only on the thickness of PEDOT:PSS. A similar effect can be observed for 700 nm light, although due the wavelength ratio of almost a factor of two, the reductions and gains for 400 nm and 700 nm light are at totally different thicknesses. Hence, under sunlight the overall gain or loss is much smaller because the interference for each wavelength is different and their effects tend to cancel. The same effects are also seen by varying ITO thickness.

Discontinuities in $\vec{E}$

Discontinuities in the electric field are not seen at normal incidence and therefore may not be expected. The continuity derives from boundary conditions established by Maxwell's Equations which require the electric field parallel to an interface to be continuous. The electric field of normal-incident and s-polarized light are always parallel to the interface and therefore always continuous. However, p-polarized light has components both parallel and perpendicular to the interface (Fig. 1). The boundary condition regarding the perpendicular electric field is that the electric displacement ($\vec{D} = \varepsilon\vec{E} = (n + ik)^2\,\vec{E}$) perpendicular to an interface is continuous (in the

absence of a free surface charge). Therefore the perpendicular components of the electric field must be discontinuous across an interface.

Increased $\vec{E}$ near Al

Interference also differs for s and p-polarized light. The electric field of s-polarized light is always normal to the plane of incidence so the incident and reflected fields are always parallel or anti-parallel to each other. For p-polarized light the electric fields are never completely aligned and therefore can never have complete constructive or destructive interference. This causes the interference pattern for p-polarized light to be more 'flat,' including near the Al interface.

Reduced effect from refraction

As light enters a medium with a higher index of refraction, the path of the light bends toward the normal. This new angle is called the angle of refraction and is also the angle of incidence at the next interface. The magnitudes of the discussed effects are highly dependent on the angle of refraction within each layer. Table 1 gives approximate angles of refraction for two angles of incidence in air. The quantity is the magnitude of both the interference pattern 'stretching' and path length increase (see below). With typical active layers of organic solar cells having n≈2, refraction is very strong, so effects are mitigated to less than 15% for all angles of incidence. It would be possible to construct a solar cell in which the angles relative to the normal inside the cell are larger, such as by using a non-planar glass substrate (such as in Ref. 5). In that case different quantitative results should be expected.

Change in reflectivity

The reflectivity of an interface changes with angle of incidence, but due to refraction only the reflectivity of the air/glass interface changes significantly. In general, reflectivity increases for s-polarized light and decreases for p-polarized light until Brewster's angle (~60° for air/glass) after which the reflectivity also increases rapidly. Therefore, planar solar cells see a sudden decrease in efficiency at angles above ~60°.

Path length increase

At oblique angles the path length of light inside a solar cell increases with $1/\cos\theta$. A longer distance traveled within the cell means more light is absorbed. However, as with the other effects the increase is reduced by refraction. As indicated in Table 1, the path length increase within P3HT:PCBM is only 15% or less compared to normal incidence.

IV. DISCUSSION

These results have implications for understanding and designing experiments. For example, Dennler et al[2] argues that improved IQE in their devices at higher angles of incidence could be explained by reduced exciton quenching at the Al interface. They make the argument that both PEDOT:PSS and evaporated electrodes are known to induce exciton quenching, but quenching at Al is probably more significant. They state that "The higher the angle, the more light is likely to be absorbed close to the ITO electrode," so more excitons will be quenched at the PEDOT:PSS interface, but less are quenched at the Al interface. Since the quenching effect is stronger for aluminum the net effect is less quenching, which explains the improved IQE.

Looking at the calculated electric field reveals that this is not a satisfactory explanation. Figure 2.4 shows the electric field inside a solar cell with the structure of the 'thin' cell from Ref. 2 at the wavelength 430 nm which showed a large increase in IQE with increasing angle of incidence. Only excitons which are generated within the exciton diffusion length (~10nm for P3HT, ~40nm for PCBM[14]) of an interface are likely to be quenched. Increasing the angle of incidence has the opposite effect than was predicted by Ref. 2, that is, the electric field actually increased at the Al interface and decreased near the PEDOT:PSS interface, even though the mean location of exciton generation was shifted slightly towards the ITO electrode. The increase in electric field at Al can be explained by the p-polarized light having only partially destructive interference, the reduction at PEDOT:PSS is due to the expansion of the interference pattern 'pushing' the electric field peak out of the active layer. So reduced exciton quenching at the

PEDOT:PSS interface, not the Al interface, is a possible explanation for the observed increase in IQE.

Understanding of the electric field inside a solar cell is helpful for interpreting results, but it could also enable new research. In a recent study using optical modeling to explore interfacial effects on efficiency,[15] an inverse relationship was found between external quantum efficiency (EQE) and $\left|\vec{E}\right|^2$ at the PEDOT:PSS/P3HT:PCBM interface. The effect was attributed to a 'reduced generation zone' where exciton dissociation is inefficient near the PEDOT:PSS interface which the authors believe is 'the dominant electrical loss for thin devices.' In their research optical modeling was used to determine $\left|\vec{E}\right|^2$ at the PEDOT:PSS interface and experimental data was acquired by fabricating cells with various active layer thicknesses and measuring EQE at different wavelengths. In this way, data was obtained for a wide range of electric field intensities at the PEDOT:PSS interface. Using the knowledge presented in this paper, studies such as this one could be extended or improved as follows. Firstly, by varying angle of incidence the electric field at the PEDOT:PSS interface could be varied for single devices, so EQE vs. $\left|\vec{E}\right|^2$ could be compared with data from a single device which would eliminate possible errors due to variations in device quality, and would reduce the need to fabricate many cells of various thicknesses. Second, probing the cathode interface would also be possible. The reduced generation zone was not observed near the Ca/Ag cathode for most wavelengths because the field drops to near zero there. The field at the cathode cannot be controlled by changing layer thicknesses. By using p-polarized light at oblique incidence the irradiance would remain high near the cathode allowing the reduced generation effect to be detected and studied.

V. CONCLUSION

We have investigated the optical electric field distribution within an organic solar cell for non-normally incident light. The distribution changes with respect to normal incidence in several interesting ways, namely, the interference pattern expands, creating more distance between nodes and antinodes, p-polarized light exhibits smaller interference minima and maxima, increasing the electric field near the cathode, and the electric field from p-polarized light is discontinuous across interfaces. Applications to current research were discussed.

ACKNOWLEDGMENTS:

The authors are grateful for fruitful discussions with K. Weninger (NCSU) and D. Aspnes (NCSU) and for ITO provided by ShinAn SNP (Korea). Work supported by the U. S. Department of Energy (DE-FG02-98ER45737).

Table 2.1. Approximate values for n, θ, and $1/\cos\theta$ in each material for angles of incidence in air of 60° and 90°. Actual values vary with wavelength.

Material	n	60° incidence in air		90° incidence in air	
		θ	$1/\cos\theta$	θ	$1/\cos\theta$
Air	1	60°	2	90°	∞
Glass, PEDOT:PSS	1.5	35°	1.22	42°	1.34
ITO, P3HT:PCBM	2	26°	1.11	30°	1.15

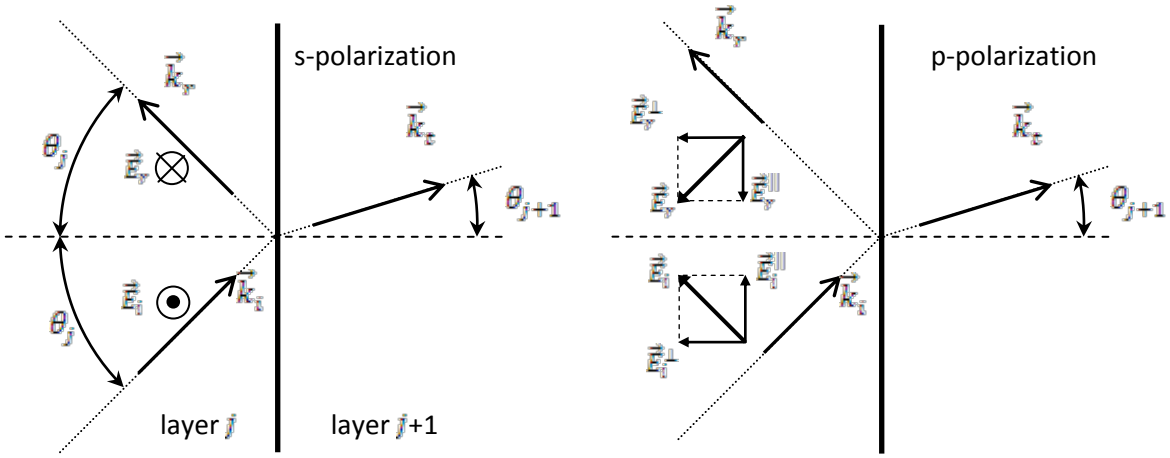

Figure 2.1. Reflection and refraction at an interface between layer j and j+1 showing the wave vectors ($\vec{k}$), associated electric field vectors ($\vec{E}$), and angles with respect to the interface normal (θ).

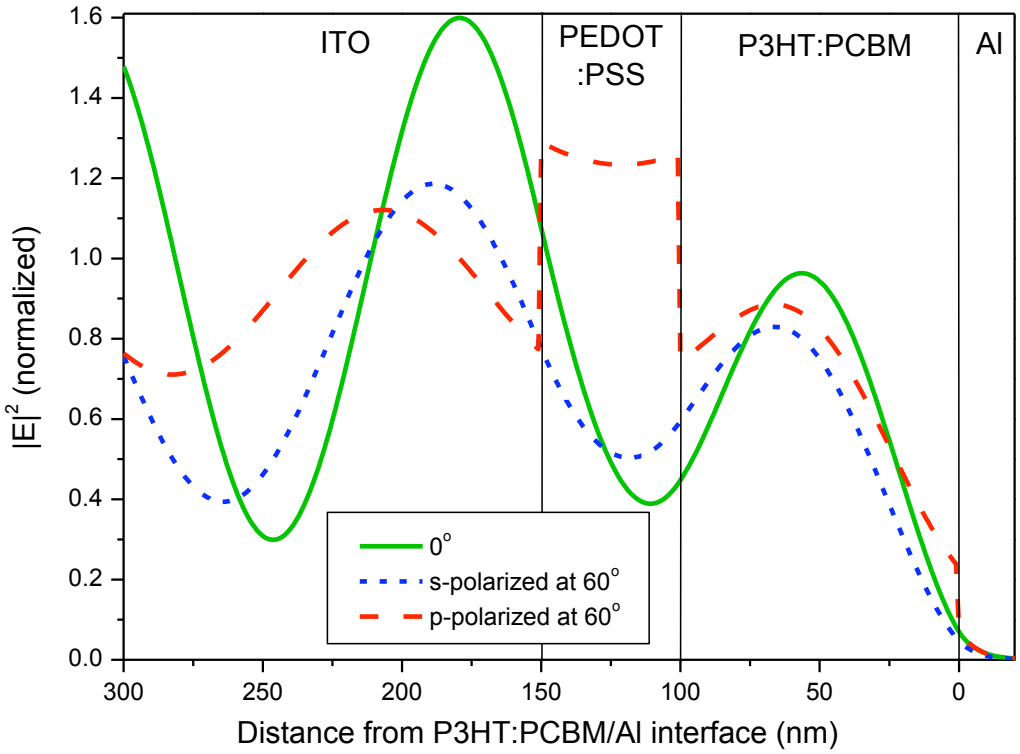

Figure 2.2. (Color online) Simulation of $\left|\vec{E}\right|^2$ inside a solar cell for 500nm light at 0°, 60° s-polarized, and 60° p-polarized light. The solar cell has structure: glass / ITO (150nm) / PEDOT:PSS (50nm) / P3HT:PCBM (100nm) / Al (100nm). $\left|\vec{E}\right|^2$ is normalized to an incident irradiance of 1 (arbitrary units) at the air/glass interface.

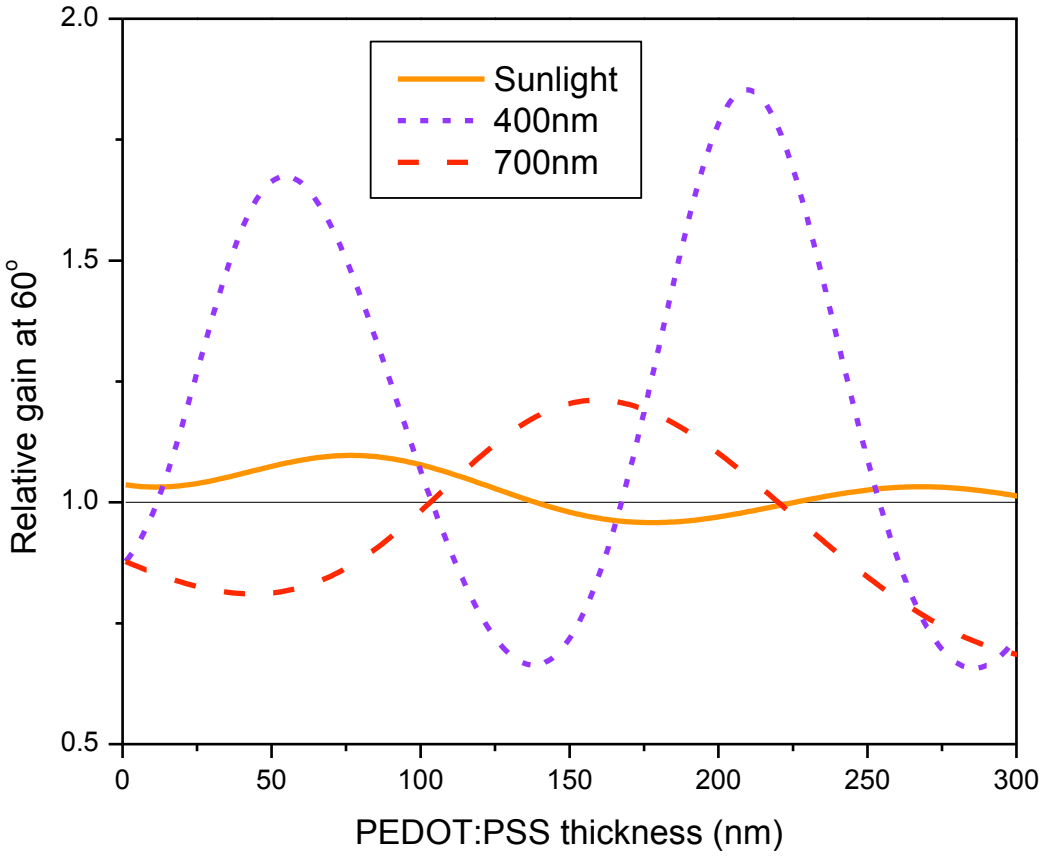

Figure 2.3. (Color online) Relative gain for 60° vs. normal incidence for a solar cell with structure: Glass / ITO (150 nm) / PEDOT:PSS / P3HT:PCBM (100 nm) / Al (100 nm) under 400 nm, 700 nm, and AM1.5G light.

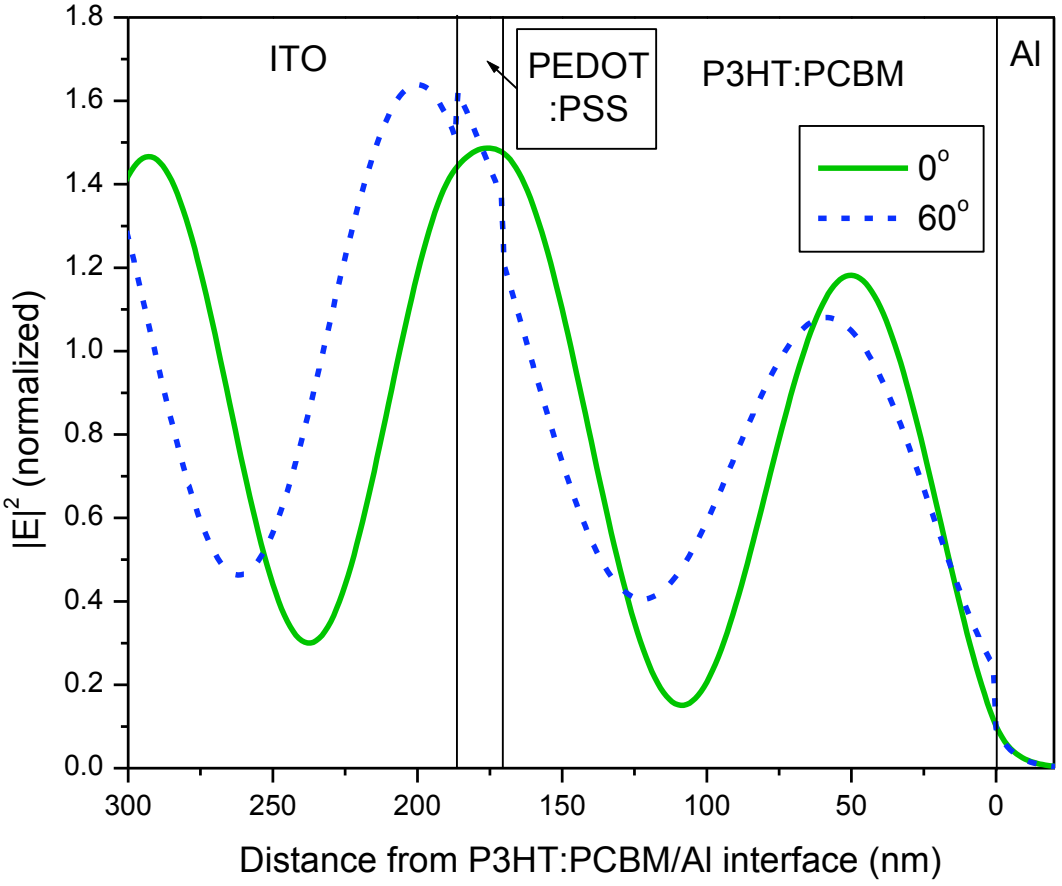

Figure 2.4. (Color online) $\left|\vec{E}\right|^2$ of 430 nm light at 0° and 60° for the 'thin' solar cell in Ref. 2, normalized to total absorption in the active layer. At this wavelength Ref. 2 (FIG. 6(c)) reported a an improvement in IQE from ~76% at 0° to ~96% at 60°.

References

[1] G. Dennler, K. Forberich, T. Ameri, C. Waldauf, P. Denk, C. J. Brabec, K. Hingerl, and A. J. Heeger, Journal of Applied Physics 102, 123109-6 (2007).

[2] G. Dennler, K. Forberich, M. C. Scharber, C. J. Brabec, I. Tomis, K. Hingerl, and T. Fromherz, Journal of Applied Physics 102, 054516-7 (2007).

[3] L. H. Slooff, S. C. Veenstra, J. M. Kroon, D. J. D. Moet, J. Sweelssen, and M. M. Koetse, Applied Physics Letters 90, 143506-3 (2007).

[4] F. Monestier, J.-J. Simon, P. Torchio, L. Escoubas, F. Flory, S. Bailly, R. de Bettignies, S. Guillerez, and C. Defranoux, Solar Energy Materials and Solar Cells 91, 405-410 (2007).

[5] M. Niggemann, M. Glatthaar, P. Lewer, C. Müller, J. Wagner, and A. Gombert, Thin Solid Films 511-512, 628-633 (2006).

[6] D. Cheyns, B. P. Rand, B. Verreet, J. Genoe, J. Poortmans, and P. Heremans, Applied Physics Letters 92, 243310-3 (2008).

[7] S.-B. Rim, S. Zhao, S. R. Scully, M. D. McGehee, and P. Peumans, Applied Physics Letters 91, 243501-3 (2007).

[8] Y. Zhou, F. Zhang, K. Tvingstedt, W. Tian, and O. Inganas, Applied Physics Letters 93, 033302-3 (2008).

[9] L. A. A. Pettersson, L. S. Roman, and O. Inganas, Journal of Applied Physics 86, 487-496 (1999).

[10] D. L. Windt, Computers in Physics 12, 360-370 (1998).

[11] M. Born and E. Wolf, *Principles of optics : electromagnetic theory of propagation, interference and diffraction of light* (Pergamon Press, Oxford ; New York, 1980).

[12] E. D. Palik and G. Ghosh, *Handbook of optical constants of solids* (Academic Press, San Diego, 1998).

[13] L. A. A. Pettersson, S. Ghosh, and O. Inganäs, Organic Electronics 3, 143-148 (2002).

[14] P. Peumans, A. Yakimov, and S. R. Forrest, Journal of Applied Physics 93, 3693-3723 (2003).

[15] A. J. Moulé and K. Meerholz, Applied Physics B: Lasers and Optics 92, 209-218 (2008).

CHAPTER 3

General method for assessing the potential of folded organic solar cells

A. Meyer and H. Ade

Department of Physics, North Carolina State University, Raleigh, NC 27695

Organic solar cells are limited to active layer thicknesses much thinner than is optimal for light absorption. To increase absorption, the promising folded solar cell light trapping structure has been investigated but not yet been fully explored. In this paper we introduce a general method for using simple optical modeling to predict the ultimate potential of the folded architecture for a given material system. However, some of the limited empirical data for the folded structure does not agree with the results of the model. Possible reasons for the difference are explored. We find a likely cause of error to be optical effects resulting from substrate thickness.

I. INTRODUCTION

Organic solar cells are limited to active layer thicknesses much thinner than is optimal for light absorption. One promising solution to this limitation is a corrugated or folded geometry that creates multiple reflections to increase absorption. Such cells have shown substantial gains over planar cells in both experiments and simulations.[1,2,3] Rim et al[1] analyzed cells of different types and described general guidelines for which cells could gain the most, namely that materials which have weaker absorption and/or are limited to thinner layers stand to gain the most from the folded structure.

As folded solar cells are a relatively novel, published work has focused on proving that the folded structure has great potential rather than on a detailed analysis. Though both modeling and experiment have been performed, both have focused on comparing the performance of single cells at various folding angles, with little comparison between experiment and theory. The most detailed theoretical analysis of the folded structure so far is a recent paper comparing planar and folded tandem cells.[4]

Until now, a means to assess the ultimate potential of the folded structure for single junction cells has not been published. In this work, we apply optical modeling to optimize cells in the folded structure and estimate expected gains for P3HT:PCBM bulk heterojunction and CuPc/C_{60} bilayer cells as examples of their respective cell types. Though our analysis is based on simple and well-established optical modeling, our results do not agree with some published experimental data or our own experimental results. We investigate possible reasons for the discrepancy between model and experiment and find likely errors resulting from neglecting the effects of substrate thickness as well as other potential sources of error.

II. THEORETICAL METHODS

Theoretical calculations were performed with the transfer matrix method (TMM).[1,5] The folded geometry was simulated by using reflected photons from one reflection as the incident photons for the next. In this way TMM was easily adapted for simulating folded solar cells for folding angles giving a whole number of reflections (i.e. 180°, 90°, 60°,… giving 1, 2, 3,… reflections). The code was written in Mathematica and verified in the planar structure by comparison to published results[6,7] and to transmission measurements.

Modeling of exciton diffusion in CuPc/C_{60} bilayers was performed with the diffusion equation.[8] Perfect exciton quenching was assumed at the CuPc/C_{60} interface and no quenching at the PEDOT:PSS/CuPc or C_{60}/BCP interfaces. Exciton diffusion lengths were taken to be 40 nm in C_{60};[9] various values were used for CuPc to demonstrate the effects of diffusion length.

Optical constants for Al, CuPc, C_{60}, and BCP were taken from references [10], [8], [8] and [11], respectively. Optical constants for glass, indium tin oxide (ITO), titanium oxide (TiOx), poly(3,4-ethylenedioxythiophene) poly(styrenesulfonate) (PEDOT:PSS), and poly(3-hexylthiophene):phenyl-C61-butyric acid methyl ester (P3HT:PCBM) were determined by fits to transmission measurements using the optical constants in Ref [7] as a starting point when appropriate. Films of PEDOT:PSS (Baytron P) and P3HT:PCBM (Sigma Aldrich : Nano-C) were spun cast on microscope glass slides at different spin rates to achieve films with different thicknesses. P3HT:PCBM films were annealed for 10 minutes at 110°C. ITO was supplied by ShinAn SNP. The optical constants for solar cells substrate glass (soda lime) differ from that of microscope slide glass (borosilicate). To determine solar cell glass constants, the ITO was etched completely away for transmission measurements. It was found that the substrate glass was more absorbing above $\lambda > \sim 600$nm, which can be seen as a blue-green tint when looking at the substrate edge-on. TiOx was prepared as described in Ref. [12]. Transmission data for all samples was acquired at normal and 60° incidence using a Cary 50SE spectrophotometer. Optical modeling (TMM) of single layers was performed using Mathematica. Results from modeling were compared to the transmission data. Literature values of the optical constants for PEDOT:PSS gave good fits to the optical transmission measurements, so the literature values

were used for PEDOT:PSS. For glass, ITO, TiOx, and P3HT:PCBM the constants were fit to our transmission data but did not vary significantly from the original constants.

III. RESULTS AND DISCUSSION

Optical modeling is often used to optimize layer thicknesses in devices. Modeling of bulk heterojunction solar cells predicts photocurrent local maxima with layer thicknesses around 80 nm and 210 nm which have been verified experimentally.[13,14] Tandem cells are also modeled to maximize efficiency.[15] Recently, this approach was used to compare planar tandem cells to folded tandem cells,[4] but until now it had not been applied to the simpler single junction folded cells.

In order to optimize the folded structure, the absorption in the active layer for different thicknesses and folding angles was calculated. Figure 3.1 shows maximum theoretical I_{SC} vs. P3HT:PCBM thickness for a planar cell and various folding angles. The model predicts a large gain for a folding angle of 90° with smaller additional gains for decreasing angles. It is evident from the graph that the best active layer thicknesses for planar cells may not be best for folded cells and that comparing cells of a single thickness at different folding angles does not provide the whole picture. For 80 nm P3HT:PCBM cells a gain of 20% is expected with folding angle $2\alpha=45°$ while at 130 nm a gain of 55% is expected. A more realistic comparison would be between, for example, a 80 nm planar cell and a 114 nm folded cell, which would give 27% improvement.

The situation looks quite different for bilayer cells, which are more limited by the exciton diffusion length. Figure 3.2 shows the predicted short circuit current of CuPc/C_{60} bilayer cells with values for the exciton diffusion length in CuPc of 5, 20, and 60 nm. In this case, the optimum CuPc thicknesses for planar and folded cells are almost identical, with folded cells having slightly thinner layers. BCP layer thicknesses used in this simulation were optimized for planar cells; absorption in the folded cells would be further increased by using thicker BCP

layers. A full analysis of this bilayer structure would include simultaneous optimization of CuPc, C_{60}, and BCP layer thicknesses, which were not performed here.

Another technique that has been used to increase absorption in very thin cells is the optical spacer layer (optical spacing is also one function of an exciton blocking layer). When an optical spacer layer and folded architecture are used together they can give enormous benefit to cells with thin layers. Figure 3.3 shows BHJ planar and folded cells with and without a 50 nm TiOx spacer layer. The spacer layer does not increase absorption for all active layer thicknesses in either the planar or folded structures, but it does help thin layers. In fact, the folded cell with S.L. absorbs more light at 30 nm than the planar cell without S.L. absorbs with any thickness less than 165 nm. The spacer layer and folding combo could be a boon to cells with poor transport properties. Note our optical constants for TiOx are lower than those used in Ref. X, so our 50 nm spacer layer would be equivalent to ~30 nm using their constants.

Our attempts to find agreement between simulated and experimental data were not as successful as hoped. Our own cells (data not shown) gained in the folded structure, but the magnitude of the experimental gains were not consistent with the model. Also, published results from Rim et al [1] do not agree with our model. It is unlikely that the discrepancy is due to an error in the simulation, since plane wave modeling is simple, well established, and successful in modeling organic solar cells. Also, our model agrees with published simulation results and our own transmission measurements at normal and non-normal incidence. However, there are aspects of the folded structure and specific experimental setups that are not included in the model. In order to determine which, if any, are likely to explain the different results we will closely examine the possible differences and compare their effects to the experimental data.

Rim et al gives experimental results for P3HT:PCBM cells of 3 different thicknesses at multiple folding angles, shown here in Figure 3.4 along with our predicted gains. In general the experimental data peaks with folding angle ~40° with higher gain than the model, then drops for angles <20°. Though Rim et al did not compare their P3HT:PCBM data to a model, the sudden drop in current at small angles was unexpected and was attributed to optical anisotropy in

P3HT:PCBM films. However, the anisotropy cited was achieved using a special technique to align the polymer chains.[16] Even if significant anisotropy did exist, it should not dominate absorption in the folded structure because many bounces occur at various angles of incidence. For example with a folding angle of 20° there would be 9 reflections having angles of incidence 80°, 60°, 40°, 20°, and 0°. Another explanation is required.

Potential errors can be sorted into two categories: those intrinsic to the folded structure and those specific to the experimental setup. Intrinsic to the structure are uneven illumination and variation in absorption vs. depth in the active layer. It is known that the folded structure creates a concentrating effect, where light is concentrated near the bottom of the 'V'. Optical modeling can calculate the degree of this effect, which can be quite strong (see ref. [17]). However, it does not count for the effects of uneven incident irradiance on device performance. For that, modeling of device physics would be required. Experimentally, Refs. [1,2] both observed a decrease in V_{OC} at small angles, with Ref. [2] also observing an increase in FF; however, the variations were small.

Another variation that can occur is in the distribution of absorbed photons within each layer. This is to say at what depth inside the active layer excitons are generated. Most optical modeling ignores any effects these may have and assumes that each absorbed photon contributes equally to current regardless of where it is absorbed, one exception being the modeling of exciton diffusion in bilayers, which does consider the absorption profile. The effect of absorption vs. depth in the active layer on internal quantum efficiency (IQE) and other device characteristics is a question relevant to all organic solar cells that has not been fully investigated for BHJ devices. Moule et al [14] showed that BHJ cells with different active layer thicknesses had different optimum P3HT:PCBM ratios, possibly due to the need to balance charge transport. In addition, Ref. [18] found that increased absorption near the PEDOT:PSS/P3HT:PCBM interface was strongly correlated with lower IQE for the overall device. The absorption profile changes significantly with angle of incidence as we detailed in a separate article. To show an example of how the absorption can vary inside a folded device, the distribution for a cell with a 115 nm P3HT:PCBM layer is shown in Figure 3.7. At a 60° folding angle, light strikes the first face with 60° incidence, then hits the second face at 0° incidence but is concentrated on the bottom half only.

The light is then reflected back to the first side for the last reflection. This creates two regions on the device, the bottom half which is struck by all three reflections, and the top half which only get the first and third. Though the absorption profiles are different, the differences are usually small and could only account for large discrepancies between experiment and model if the device is highly sensitive to the absorption profile.

There are also differences between the actual experimental structure of a folded solar cell and what has been modeled, some of which have been noted in the literature. A simple optical model assumes that the structure is a perfect V (Fig. 3.5a), and light enters through an opening with width $2\ell\cos\alpha$, where ℓ is the length of the active layer along one face of the V. A close examination reveals many differences between this idealization and a real experiment. The following discussion analyzes the folded structure made by two planar cells held together at an angle as in Refs [1,2]. Cells made by a patterned substrate such as in Ref [3] would require a different analysis.

There are several fairly obvious errors that an experimenter would likely notice and attempt to minimize. If the active area did not cover the entire substrate then light from outside the intended area could reflect onto the active area, increasing measured gain (Fig. 3.5b). If there were a gap between the two faces, reflected light would escape out the bottom (Fig. 3.5b). Also, the two individual cells may not have active areas reaching to the bottom edge of the substrates, and the two opposing faces may not be perfectly aligned with each other. These errors will not be further discussed here.

More subtle errors may occur which are caused by using a thick substrate. These errors are worth considering since substrate thicknesses are in the range of 0.3-1.0 mm, and active area dimensions are on the order of millimeters, as depicted in Figure 3.5c. Specific errors will vary with the experimental setup, but likely ones are shown in Figure 3.5d-g and discussed below.

At the top of the V, several different errors are possible depending on the setup. Light could either be allowed to enter through the end of the substrate (Fig. 3.5f), or it could be blocked (Fig.

3.5g). If the end were opaque then no extra light would enter, but there would be a shaded region where the active area is totally unilluminated. The shading does not reduce the total light absorbed relative to the model, as that is defined by the area of incident light, but it does contribute to uneven illumination over the active area.

Light penetrating the substrate face will exit the substrate at further down the face than in entered due to travelling within the substrate (Fig. 3.5d). Though this displacement does not cause any errors directly, it further increases the concentration already present at the bottom of the V. The type of modeling used in Ref. X may account for this effect, but not as it was used, since the layer structure used did not include a substrate layer.

Though it may appear that light is lost out the bottom of Figure 3.5c, no light will be lost since any light entering from the substrate face will be totally internally reflected off the bottom (for substrates with index of refraction $n < \sqrt{2}$ there may be some loss). However, after being reflected off the bottom, the light will be lost out of the top without completing the full number of reflections (see Figure 3.5e). The effect of reflecting off the bottom is to reverse the direction of the path of light, so light striking the bottom on its first pass will be reflected directly out. Light striking the bottom on the second bounce will be sent back for one additional pass, giving a total of three bounces. Any light incident within $2t\tan\varphi$ of the bottom will only strike the active area one time before being reflected out of the 'V', where φ is the angle of refraction in the substrate as in Fig. 3.5d, and t is the substrate thickness. As folding angle decreases the importance of this effect increases, since concentration causes more light to strike within $2t\tan\varphi$ of the bottom of the V, and a higher number of would-be bounces are lost when light is ejected early. Also as angle of incidence increases past 60° the reflectivity of the air/glass interface increases rapidly, meaning more light that does strike the solar cell face is reflected off the substrate surface and does not reach the active layer, making subsequent bounces more important.

Since the magnitudes of these errors are highly dependent on the ratio of substrate thickness to active area length, the easiest way to reduce the errors is to use a large active area on a thin substrate. Ref. [2] uses a thin (0.25 mm) substrate with active area of length ~5mm, giving a 1:20 ratio. Ref. [1] uses active area of 2.4-3.2 mm^2 with a glass substrate of unspecified thickness. Assuming the substrate thickness to be 0.7 mm (common for glass substrates with ITO), and the active area geometry to be square, the substrate-to-active length ratio would be ~1:3. Figure 3.6 shows what effect the substrate:active area ratio has on the amount of incident light that is prematurely reflected out the top as shown in Figure 3.5e. Up to folding angle $2\alpha = 18°$, a given light ray could undergo 1, 3, 5, or the maximum # of bounces. At $2\alpha = 18°$, for a 1:20 ratio 80% of incident light goes through a full 10 passes. However, for a 1:4 ratio, 100% of incident light is reflected early. The similar shape of the curves in Fig. 3.6b and the experimental data in Fig. 3.4 suggests reflection off the bottom of the V is a likely explanation for the observed drop in efficiency.

We have introduced a general method for using simple optical modeling to predict the ultimate potential from the folded architecture for a given material system. Before the model can be relied upon, however, it must be reconciled with experimental data. We have identified likely and less likely reasons for current disagreements between theory and experiment. Many of the potential problems are due to substrate thickness and could be minimized experimentally. Alternately, optical modeling could be altered to include these effects. Predicting the effects of uneven light intensity on and within the active layer would require modeling the relevant devices physics; the results of such modeling would apply to organic solar cells in general.

ACKNOWLEDGMENTS:

The authors are grateful for ITO provided by ShinAn SNP (Korea). Work supported by the U. S. Department of Energy (DE-FG02-98ER45737).

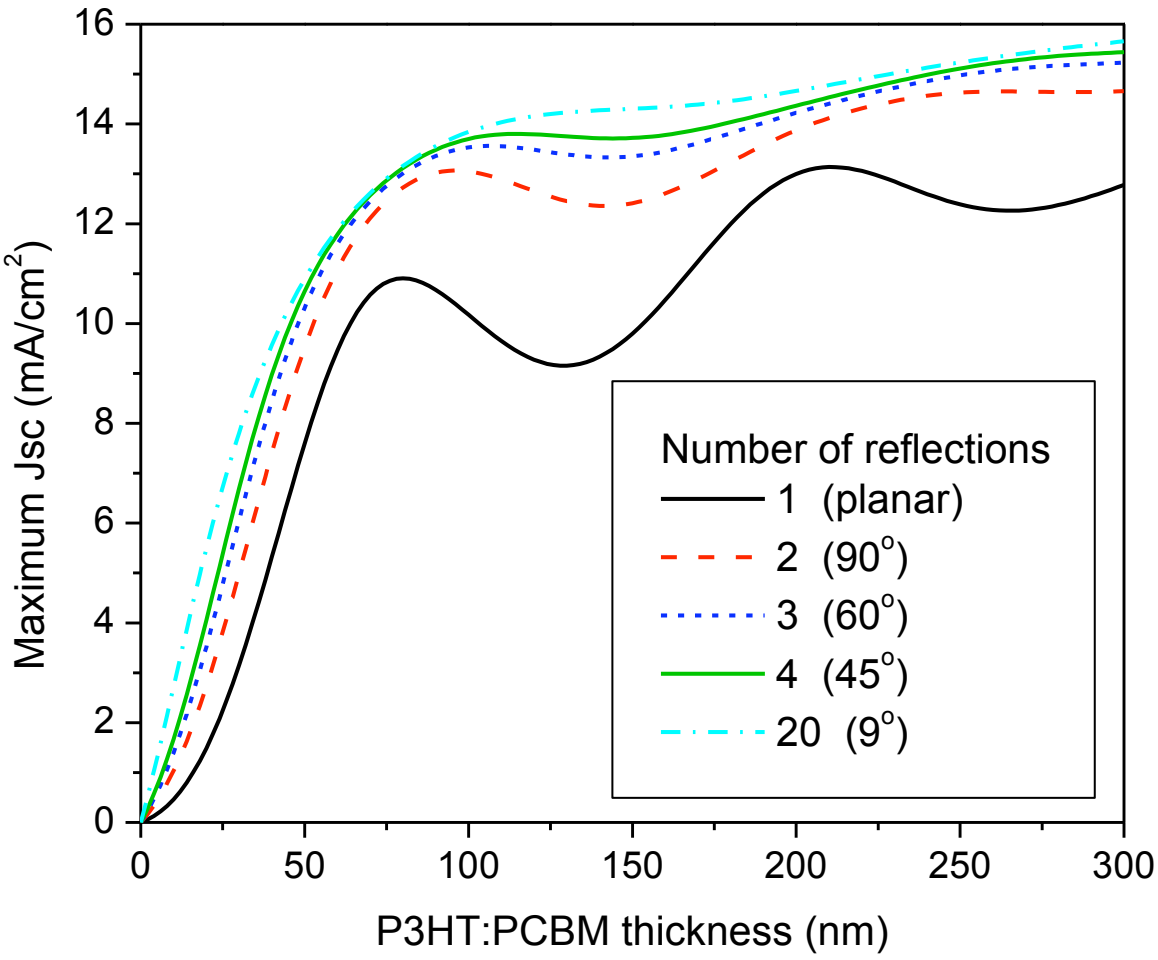

Figure 3.1. (Color online) Theoretical Jsc vs active layer thickness for cells with the structure: ITO (140nm) / PEDOT:PSS (30nm) / P3HT:PCBM / Al (100nm) with various folding angles.

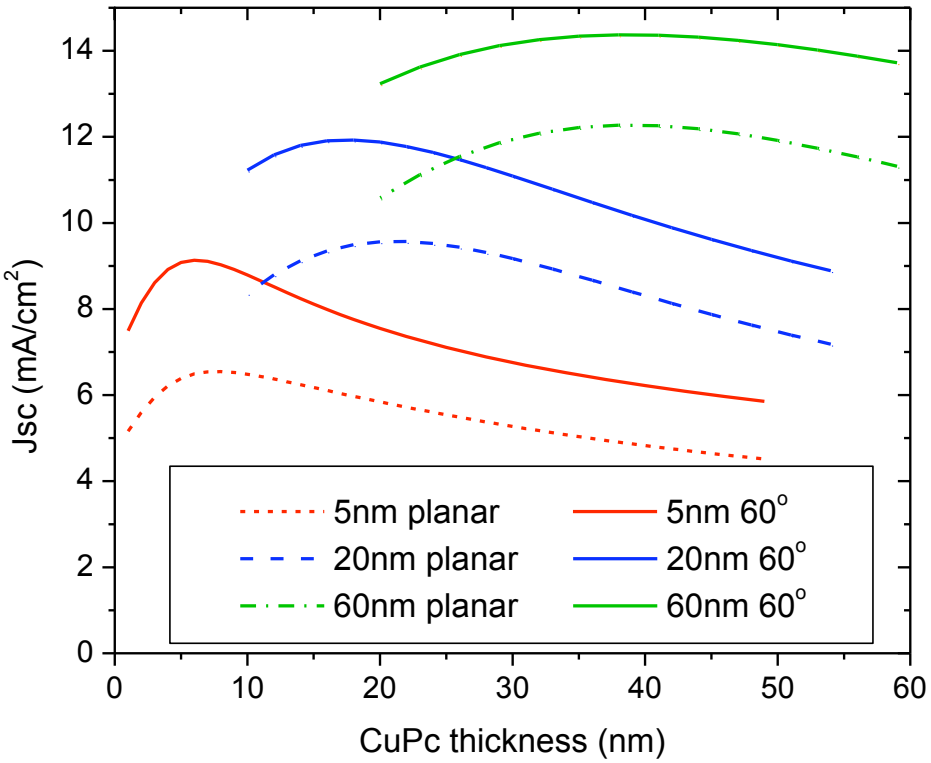

Figure 3.2. (Color online) Theoretical Jsc vs active layer thickness for cells with the structure: ITO (140nm) / PEDOT:PSS (30nm) / CuPc / C_{60} (40 nm) / BCP / Al (100nm) in planar and 60° folded configurations with exciton diffusion lengths of 5, 20, and 60 nm. BCP thicknesses were optimized in the planar structure for each diffusion length and are 20, 14, and 5 nm respectively.

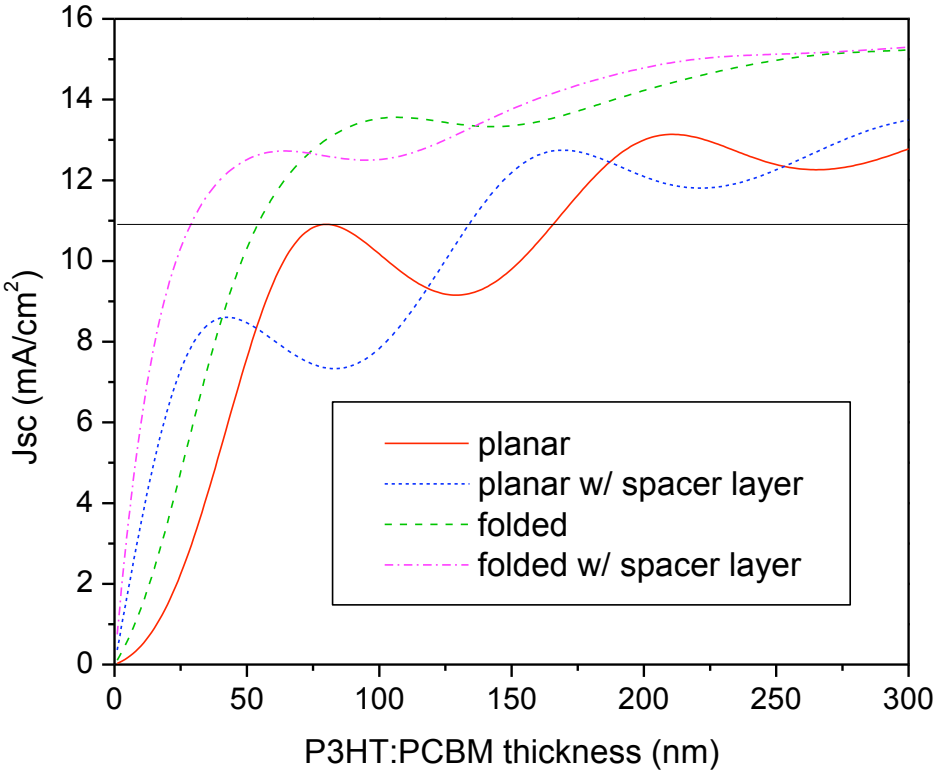

Figure 3.3. (Color online) Theoretical Jsc vs active layer thickness for cells with the structure: ITO (140 nm) / PEDOT:PSS (30 nm) / P3HT:PCBM / TiOx (0 or 50 nm) / Al (100 nm) in planar and 60° folded configurations with and without a TiOx spacer layer. The horizontal line is Jsc for the planar (no spacer layer) cell with 80 nm active layer (10.9 mA/cm^2).

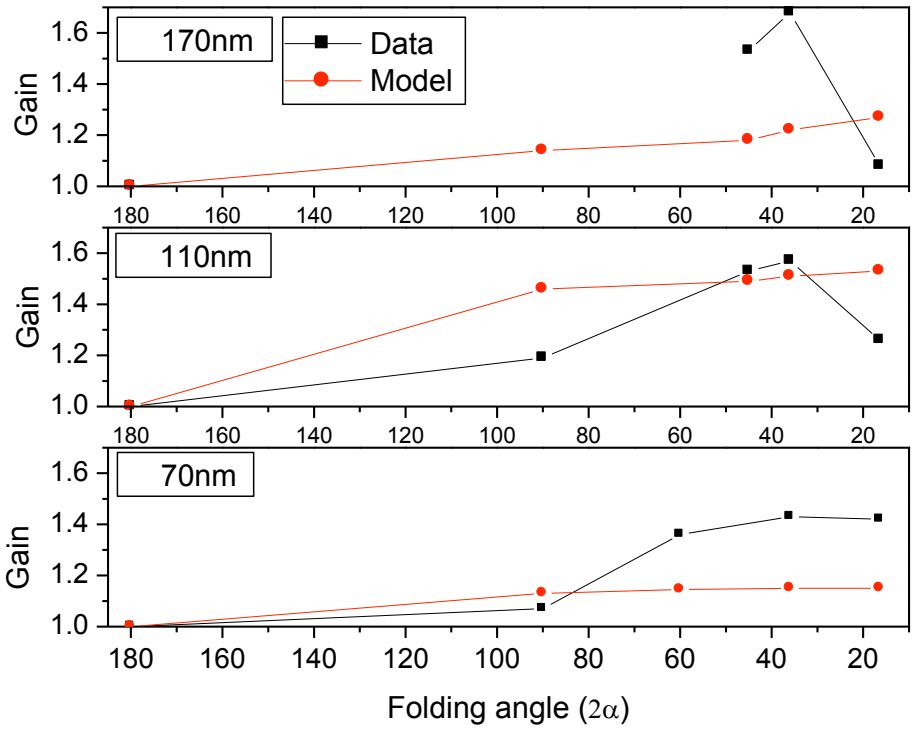

Figure 3.4. (Color online) Plot of gain (I_{SC} folded / I_{SC} planar) vs. folding angle 2α for the P3HT:PCBM cells in Ref [1]. Data is from Ref. [1], Figure 4; model is our simulation. Lines are guides for the eye.

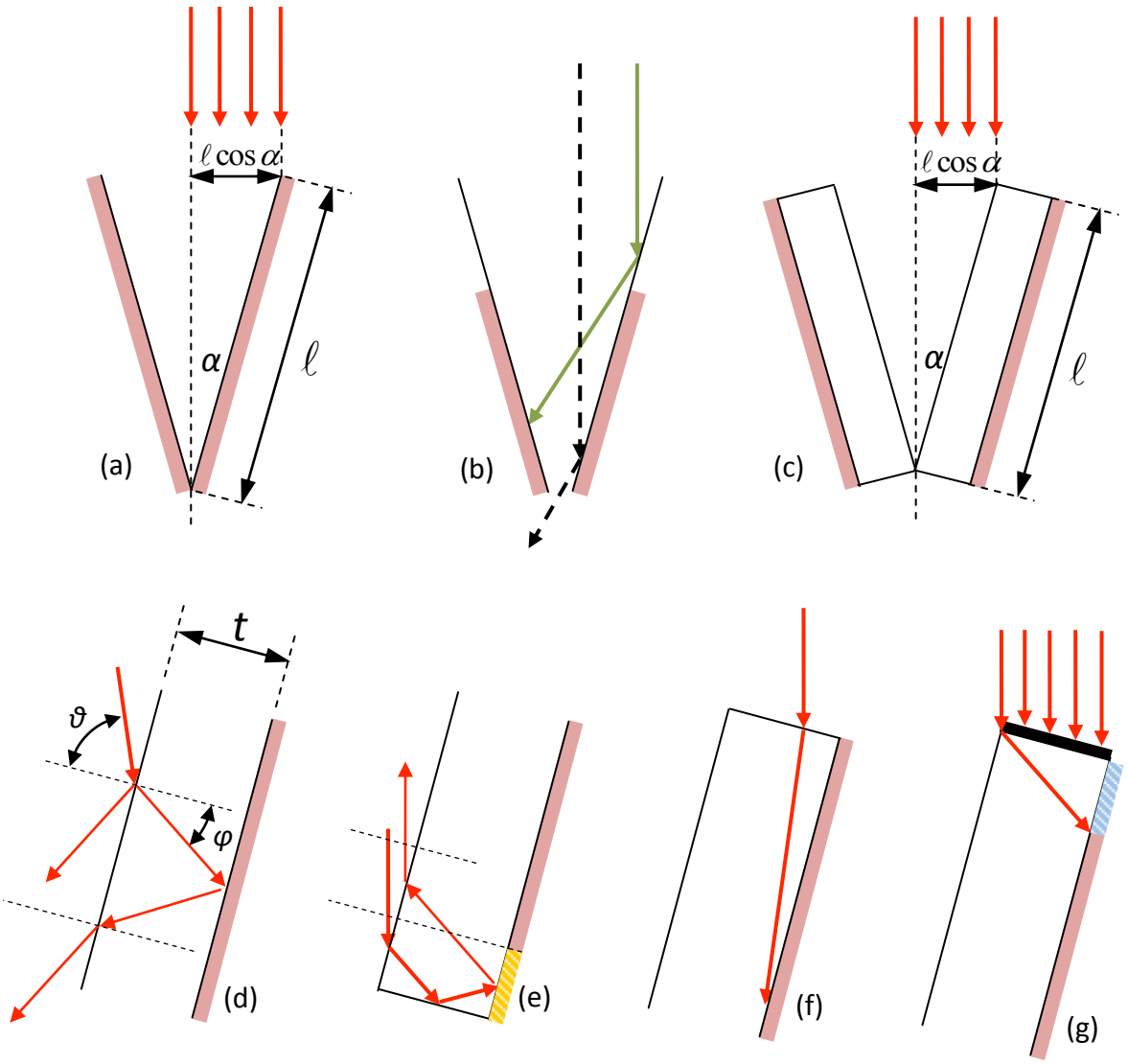

Figure 3.5. (Color online) Shaded pink denotes active areas. A folded cell as it is usually modeled (a), experimental errors that could occur (b): light reflecting from outside the active area (solid arrows), and light escaping from a gap between the two edges (dashed arrows). An actual folded cell having a substrate of finite thickness (c). light exiting the substrate is translated relative to the model due to travel within the substrate (d), light being prematurely reflected off the edge of the substrate (e), light entering through the edge of the substrate (f), and a section of the active area which receives no light (g).

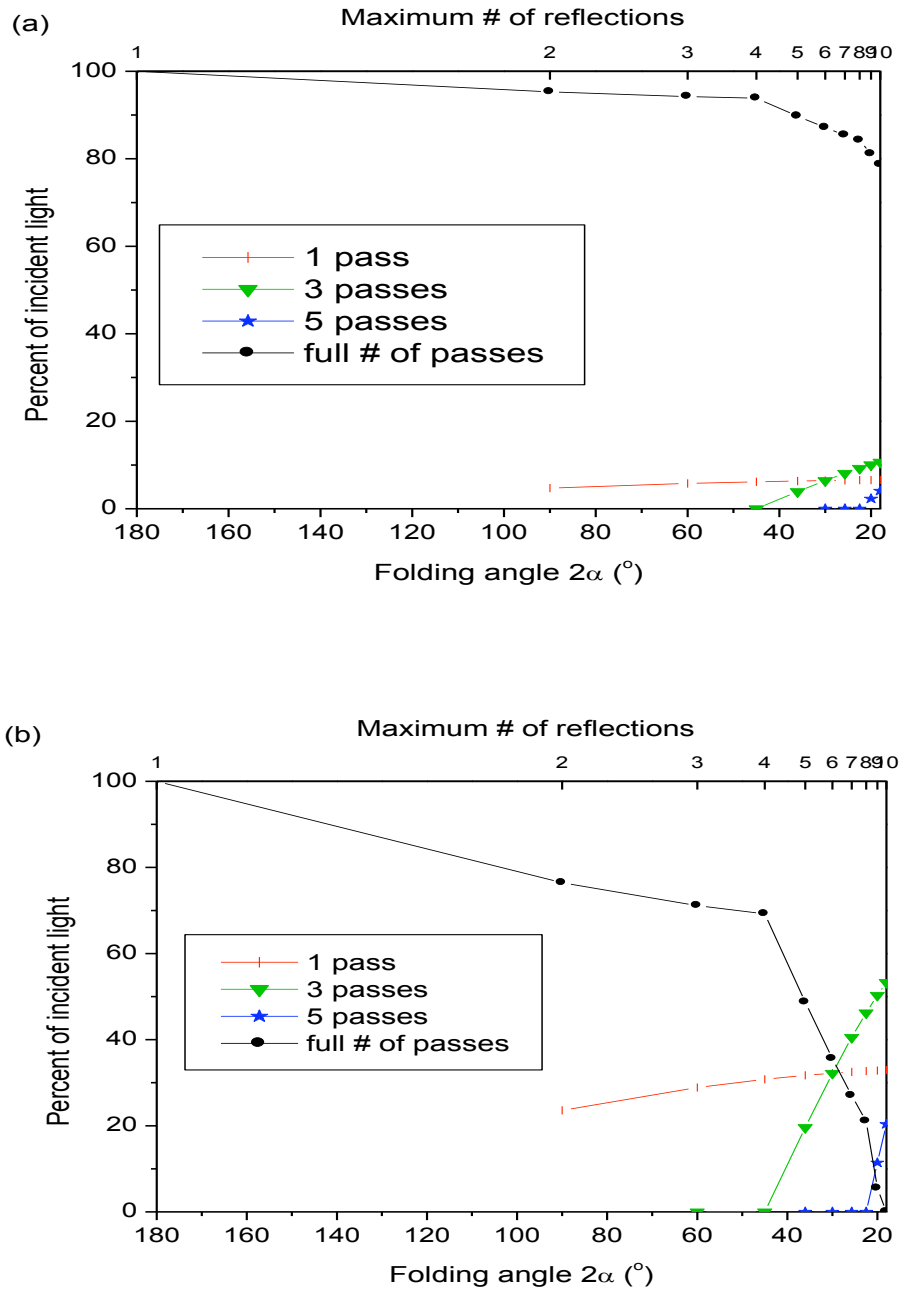

Figure 3.6. (Color online) The percentage of incident light which undergoes only 1, 3, and 5 reflections on the active layer for different folding angles, and the percentage which completes the full number of passes for substrate-thickness:active-area-length ratios of 1:20 (a) and 1:4 (b).

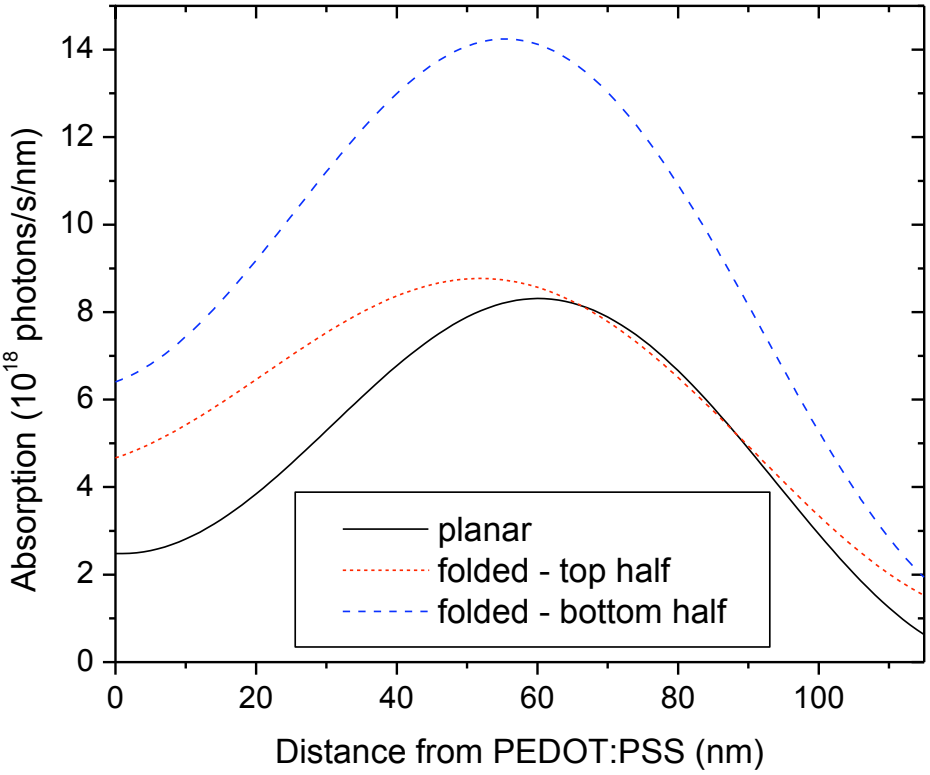

Figure 3.7. (Color online) Absorption profile for a solar cell with structure: ITO (140 nm) / PEDOT:PSS (30 nm) / P3HT:PCBM (115 nm) / Al (100 nm) in planar and 60° folded configurations under 1 sun (AM1.5G).

References

[1] Seung-Bum Rim, Shanbin Zhao, Shawn R. Scully et al., "An effective light trapping configuration for thin-film solar cells," Appl. Phys. Lett. **91** (24), 243501-243503 (2007).

[2] Yinhua Zhou, Fengling Zhang, Kristofer Tvingstedt et al., "Multifolded polymer solar cells on flexible substrates," Appl. Phys. Lett. **93** (3), 033302-033303 (2008).

[3] M. Niggemann, M. Glatthaar, P. Lewer et al., "Functional microprism substrate for organic solar cells," Thin Solid Films **511-512**, 628-633 (2006).

[4] B. Viktor Andersson, Nils-Krister Persson, and Olle Inganas, "Comparative study of organic thin film tandem solar cells in alternative geometries," J. Appl. Phys. **104** (12), 124508-124506 (2008).

[5] Leif A. A. Pettersson, Lucimara S. Roman, and Olle Inganas, "Modeling photocurrent action spectra of photovoltaic devices based on organic thin films," J. Appl. Phys. **86** (1), 487-496 (1999).

[6] B. Viktor Andersson, David M. Huang, Adam J. Moule et al., "An optical spacer is no panacea for light collection in organic solar cells," Appl. Phys. Lett. **94** (4), 043302-043303 (2009).

[7] Gilles Dennler, Karen Forberich, Markus C. Scharber et al., "Angle dependence of external and internal quantum efficiencies in bulk-heterojunction organic solar cells," J. Appl. Phys. **102** (5), 054516-054517 (2007).

[8] Florent Monestier, Jean-Jacques Simon, Philippe Torchio et al., "Optical modeling of organic solar cells based on CuPc and C60," Appl. Opt. **47** (13), C251-C256 (2008).

[9] Peter Peumans, Aharon Yakimov, and Stephen R. Forrest, "Small molecular weight organic thin-film photodetectors and solar cells," J. Appl. Phys. **93** (7), 3693-3723 (2003).

[10] Edward D. Palik and Gorachand Ghosh, *Handbook of optical constants of solids*. (Academic Press, San Diego, 1998).

[11] Z. T. Liu, C. Y. Kwong, C. H. Cheung et al., "The characterization of the optical functions of BCP and CBP thin films by spectroscopic ellipsometry," Synthetic Met **150** (2), 159-163 (2005).

[12] S. H. Kim J. Y. Kim, H.-H. Lee, K. Lee, W. Ma, X. Gong, A. J. Heeger,, "New Architecture for High-Efficiency Polymer Photovoltaic Cells Using Solution-Based Titanium Oxide as an Optical Spacer," Adv. Mater. **18** (5), 572-576 (2006).

[13] Gang Li, Vishal Shrotriya, Jinsong Huang et al., "High-efficiency solution processable polymer photovoltaic cells by self-organization of polymer blends," Nat Mater **4** (11), 864-868 (2005); Gang Li, Vishal Shrotriya, Yan Yao et al., "Investigation of annealing effects and film thickness dependence of polymer solar cells based on poly(3-hexylthiophene)," J. Appl. Phys. **98** (4), 043704-043705 (2005).

[14] Adam J. Moule, Jorg B. Bonekamp, and Klaus Meerholz, "The effect of active layer thickness and composition on the performance of bulk-heterojunction solar cells," J. Appl. Phys. **100** (9), 094503-094507 (2006).

[15] Gilles Dennler, Karen Forberich, Tayebeh Ameri et al., "Design of efficient organic tandem cells: On the interplay between molecular absorption and layer sequence," J. Appl. Phys. **102** (12), 123109-123106 (2007).

[16] H. G. O. Sandberg T. G. Bäcklund, R. Österbacka, H. Stubb, M. Torkkeli, R. Serimaa,, "A Novel Method to Orient Semiconducting Polymer Films," Adv Funct Mater **15** (7), 1095-1099 (2005).

[17] Viktor Andersson, Kristofer Tvingstedt, and Olle Inganas, "Optical modeling of a folded organic solar cell," J. Appl. Phys. **103** (9), 094520-094527 (2008).

[18] A. J. Moulé and K. Meerholz, "Intensity-dependent photocurrent generation at the anode in bulk-heterojunction solar cells," Applied Physics B: Lasers and Optics **92** (2), 209-218 (2008).

CHAPTER 4

Poly(3-hexylthiophene):phenyl-C61-butyric acid methyl ester bulk heterojunction solar cells with high open circuit voltage

A Meyer,[a] J Seok,[b] H Ade[a]

[a] Department of Physics, North Carolina State University, Raleigh, NC 27695

[b] Department of Materials Science, North Carolina State University, Raleigh, NC 27695

The open circuit voltage (V_{OC}) of organic solar cells is strongly correlated to the energy difference between the highest occupied molecular orbital (HOMO) of the electron donor and the lowest unoccupied molecular orbital (LUMO) of the acceptor. However, the maximum attainable V_{OC} and the loss mechanisms involved have not been precisely determined. Virtually no progress has been made in recent years toward the improvement of V_{OC} for existing material systems, with highest V_{OC} for Poly(3-hexylthiophene):phenyl-C61-butyric acid methyl ester (P3HT:PCBM) bulk heterojunction solar cells remaining around 0.65 V for high efficiency cells and ~0.7 V for unannealed cells. In this letter, we report the fabrication of P3HT:PCBM bulk heterojunction solar cells with open circuit voltage as high as 0.82 V for unannealed devices. The devices were made with an indium-gallium eutectic cathode. It was found that air exposure during processing increased shunt resistance and V_{OC} in bulk heterojunction and single material devices. The changes due to air exposure are attributed to the formation of a gallium oxide layer hole-blocking layer at the cathode interface. A more controlled way to create such an oxide layer, in conjunction with controlled morphology, might lead to record power conversion in the P3HT:PCBM system. More general, the results strongly suggest that bandstructure enginnering in organic devices in general has still room for improvements.

The power conversion efficiency (PCE) of a photovoltaic cell can be most conveniently expressed as the product of the open circuit voltage (V_{OC}), the short circuit current (I_{SC}), and the fill factor (FF). Increasing any of these three factors without reducing the other two would directly improve the PCE. In organic bulk heterojunction devices (BHJ) comprised of a donor and an acceptor semiconducting material, I_{sc} depends on absorption, film thickness, exciton splitting efficiency and charge collection efficiency, FF depends on transport properties as expressed in series and parallel resistance, and Voc depends primarily on the electronic structure, i.e. valence and conduction bands of the materials and how these align at the various interfaces. The V_{OC} of organic solar cells is strongly correlated to the energy difference between the highest occupied molecular orbital (HOMO) of the electron donor and the lowest unoccupied molecular orbital (LUMO) of the acceptor.[1] However, measurements of the HOMO and LUMO levels differ substantially, ranging from 4.8 to 5.2 eV for the HOMO of Poly(3-hexylthiophene) (P3HT)[2,3], and from 3.75 to 4.3eV for the LUMO of phenyl-C61-butyric acid methyl ester (PCBM)[3,1] In addition, the exact band alignment and band bending are not understood. [6,7,8] Therefore, estimates of the theoretical maximum V_{OC} for P3HT:PCBM devices also vary, for example: 0.8 V,[1] 1.0 V,[2,4], and 1.45 V.[3] The difference between the high and low values of these estimates would correspond to a substantial difference in PCE of ~80%, a difference that needs to be explored and understood. Presently, the highest V_{OC} realized for high efficiency devices is ~0.66 V.[9] In this letter, we report P3HT:PCBM BHJ solar cells with open circuit voltage as high as 0.82 V for unannealed cells, which is considerably higher than the highest published value of ~0.7 V (see, for example, Refs. 10,11,12).

The high V_{OC} reported was achieved using an Indium-Gallium eutectic cathode. We describe the fabrication of cells with three different active layers: P3HT, PCBM, and P3HT:PCBM BHJ and compare their performance with and without exposure to air. We find an increase in V_{OC} of 0.06-0.15 V for BHJ cells depending on the fabrication conditions. Both types of single layer cells show huge improvement in shunt resistance and V_{OC}, with the later increasing by 0.37 V and 0.64 V for P3HT and PCBM cells, respectively. In all cases, we attribute the increase to the formation of a gallium-oxide interfacial layer. In single layers, which

have inefficient exciton splitting, the V_{OC} is more sensitive to shunt resistance due to much lower photocurrent.

We used a novel procedure to fabricate encapsulated cells with Indium-Gallium eutectic cathodes. InGa eutectic, a metal which is liquid at room temperature, has been used as the cathode in organic solar cells to simplify fabrication in research[13] and in teaching labs.[14] Ref. 13 found that devices with InGa had similar performance to Al cells. To fabricate our devices, poly(3,4-ethylenedioxythiophene) poly(styrenesulfonate) (PEDOT:PSS) (Baytron P) was spun cast on top of indium tin oxide (ITO) (ShinAn SNP) and heated in air. The active layer was cast inside a nitrogen glovebox from chlorobenzene solutions of P3HT (Sigma-Aldrich), PCBM (Nano-C), or P3HT:PCBM (1:1 weight ratio). A paper hole-punch was used to make a round hole in a piece of electrical tape and the tape was placed over the active layer (sticky side down). UV-cure adhesive was placed onto the electrical tape surrounding the hole. A drop of InGa (Alfa Aesar or Sigma-Aldrich) was dispensed from a syringe onto another slide of ITO covered glass to create the cathode. The BHJ supported on the PEDOT/ITO anode were pressed together so that the InGa filled the hole in the tape and made contact with the active BHJ layer. The tape has the dual purpose of defining the active area and preventing shorts outside the active area. After curing the adhesive, the device can be treated like an encapsulated device having a solid metal cathode. Using thin ITO layers on both sides of the solar cell increases the series resistance. Since transparency is not required for the cathode side a metal could be used to contact the InGa instead of ITO. However, when this was attempted with Al the devices were unreliable because InGa causes Al to react in the presence of air to form a non-conducting compound.[15] In order to reduce the effect of high external resistance until a substitute for the ITO on the cathode side is found, small (<5 mm^2) active areas were used (giving lower resistance in Ω-cm^2). The above method provides an easy and reliable means to fabricate cells with liquid cathodes, with the notable drawback that active area size varied due to possible stretching of the tape and/or incomplete InGa contact over the covered area. The cells remain functional for many days, though some degradation did occur. The rate of degradation was not investigated. Annealing for the reported cells was always performed before depositing the InGa cathode. Annealing after

adding InGa always hugely degraded device performance. To control whether cells were exposed to air, cells were encapsulated inside the glovebox or taken outside after spin casting the active layer for depositing the InGa and encapsulation. I-V measurements were taken with a Keithley 2400 sourcemeter. Devices were illuminated with an Oriel 150W solar simulator under AM1.5G at 100mW/cm^2 calibrated using a Hamamatsu S1133 photodiode.[16]

The open circuit voltage of BHJ cells was found to be highly consistent when using the same fabrication conditions, but could vary greatly with only small changes in parameters such as solution concentration, P3HT:PCBM ratio, and spin rate. To demonstrate these phenomena, two sets of BHJ cells were made under the same conditions except for spin rate. For each set, four types of cells were made from the combinations of two parameters: unannealed/annealed (110°C for 5m), and nitrogen/air (inside or outside of a glovebox). Figure 4.1 gives I-V curves for one cell from each category, while Figure 4.2 shows the V_{OC} achieved for each type of cell. In these two data sets the effects of annealing and air exposure on the V_{OC} are relatively independent of each other, though that was not always true for our cells. The V_{OC} of 1200 RPM cells gained ~0.07 V from air exposure, while the 1500 RPM cells gained ~0.13 V.

In order to see the effect of air exposure on P3HT and PCBM individually, we investigated cells with active layers of pure P3HT or PCBM on top of PEDOT:PSS. These 'single material' cells showed limited diode and photodiode characteristics, including a small photocurrent. PCBM cells had short circuit currents ~20x greater than P3HT cells, suggesting semi-efficient exciton splitting at the PEDOT:PSS/PCBM interface. The V_{OC} of these cells is shown in Figure 4.2 and listed in Table 4.1 along with values for other important parameters. Air exposure dramatically increased Rp and V_{OC} for both types of cells while having a small effect on Rs and I_{SC}. It was found that annealing made no difference to the single material cells except to somewhat reduce series resistance in P3HT cells.

It is highly likely that the increase in V_{OC} and R_p are due to the formation of a hole-blocking oxide layer at the active layer / cathode interface. Dielectric and n-type semiconductor layers such as LiF[17] and TiO_X[18,19] have been shown to increase V_{OC} and shunt resistance in organic solar cells. Also, Zhao et al[20] found that exposing cells with Ca/Al electrodes to air

increased their V_{OC}, presumably by the formation of CaO. Gallium is easily oxidized; in air the surface of InGa eutectic primarily consists of gallium-oxide.[21] It is likely that GaO_X is present at the organic/InGa interface and is responsible for increased R_P and V_{OC}. Attributing the change in R_P to an interface is consistent with the R_P data (Table 4.1). In the dark, where R_P is dominated by charge injection, R_P for single material and BHJ cells shows huge differences between those with and without air exposure. However, for BHJ cells under bright light, when R_P is dominated by recombination in the bulk, the shunt resistance is relatively unaffected by air exposure.

The change in V_{OC} of single material cells due to air exposure can be completely explained in terms of the shunt resistance. Solving the characteristic equation of a solar cell for V under open-circuit conditions (J = 0) yields an equation for V_{OC}. The maximum V_{OC} (with infinite shunt resistance) is given by $\frac{nkT}{q}\ln(\frac{J_L}{J_0}-1)$, where n is the diode ideality factor, k is Boltzmann's constant, T is absolute temperature, q is the elementary charge, J_L is photocurrent, and J_0 is the reverse saturation current. The expected V_{OC} relative to this maximum varies with the quantity R_P x J_L as shown in Figure 4.3. For R_P x J_L > ~1 V the expected V_{OC} is relatively independent of R_P, but at lower values of R_P the V_{OC} drops off quickly. Values of R_P x J_L for our cells are listed in Table 4.1 using J_{SC} as an approximation of J_L; also listed is the expected Voc expressed as percent of maximum V_{OC} for a given J_L and J_0. For both P3HT and PCBM single layer cells there is very strong agreement between V_{OC} expected and actual V_{OC} measured. However, the same is not true for BHJ cells. R_P x J_L for BHJ cells are all relatively high; moreover, higher R_P x J_L does not correlate with higher V_{OC} for the BHJ cells. In terms of the characteristic equation, the increase in V_{OC} could be attributed to a lower J_0. Possible physical explanations are discussed below.

Typical literature values for open circuit voltages for P3HT:PCBM cells range from 0.6-0.7 V for unannealed cells and 0.55-0.65 V for annealed ones. Our InGa cells ranged from 0.44 V to 0.82 V. PCE for unannealed cells was limited to less than 1% due to poor I_{SC} and FF; annealed cells had PCE around 2%. In both cases, cells with air exposure had higher PCE. The relatively low efficiencies are attributed to poor morphology and unoptimized layer thickness,

not to the InGa electrode. In contrast, some of the variation for a given cell type are most likely due to insufficient control of the GaOx layer. Our cells with Al cathodes have similar performance ot the InGa cells. A high open circuit voltage is tantalizing, but only beneficial if it could be achieved in a cell that also has optimized morphology and thickness. Our cells with the highest PCE have V_{OC} from 0.55 to 0.65 V, which is similar to published values.

The precise nature of the gain in V_{OC} in BHJs devices is unclear. The oxide layer could be preventing shorts in devices which have pure phases connecting both electrodes, similar to the single material cells. In this case, the variability of the effect would be due to the extent of how 'shorted out' the bulk is. However, since measured VOC is not highly dependent on R_P, this is unlikely. Alternately, the oxide layer could alter the band alignment at the P3HT:PCBM/InGa interface. Variation in the effect on V_{OC} could be due to surface composition and/or morphology affecting the band alignment, which is something that has not been studied. If the surface does affect band alignment, then the V_{OC} gain could potentially be decoupled from the bulk morphology. This would allow independent optimization of V_{OC}, I_{SC}, and FF to achieve real gains in PCE.

Our results show that the maximum V_{OC} possible for P3HT:PCBM BHJ devices might not have been achieved yet. Interface band structure alignment and band structure engineering still have room for improvements and are relatively poorly understood aspects of organic device operation. The challenge will be to incorporate our observation into a device fabrication process that also optimizes the morphology and charge transport properties.

We thank J. Lewis and G. Cunningham (RTI) for support and use of RTI facilities, ShinAn SNP (Korea) for providing the ITO , and the US Departmet of Energy for support under contract DE-FG02-98ER45737.

Table 4.1 Values of device parameters for cells made under various conditions. J_{SC} was used as an estimate of J_L.

Cell	Exposure	Anneal	Dark R_P (Ω-cm^2)	Light R_P (Ω-cm^2)	V_{OC} (V)	Jsc (mA/cm^2)	R_P x J_L (V)	V_{OC} (% $V_{OC,max}$)
PCBM	N_2	-	22	19	0.005	0.28	0.01	1.4%
	air	-	38000	7500	0.65	0.20	1.51	96%
P3HT	N_2	-	4100	3300	0.06	0.01	0.05	7%
	air	-	290000	76000	0.43	0.01	0.54	74%
BHJ (1500 RPM set)	N_2	N	6100	760	0.74	1.78	1.35	95%
	N_2	Y	1900	480	0.49	4.34	2.08	97%
	air	N	750000	740	0.80	2.31	1.71	96%
	air	Y	1500000	1100	0.58	3.60	3.96	99%

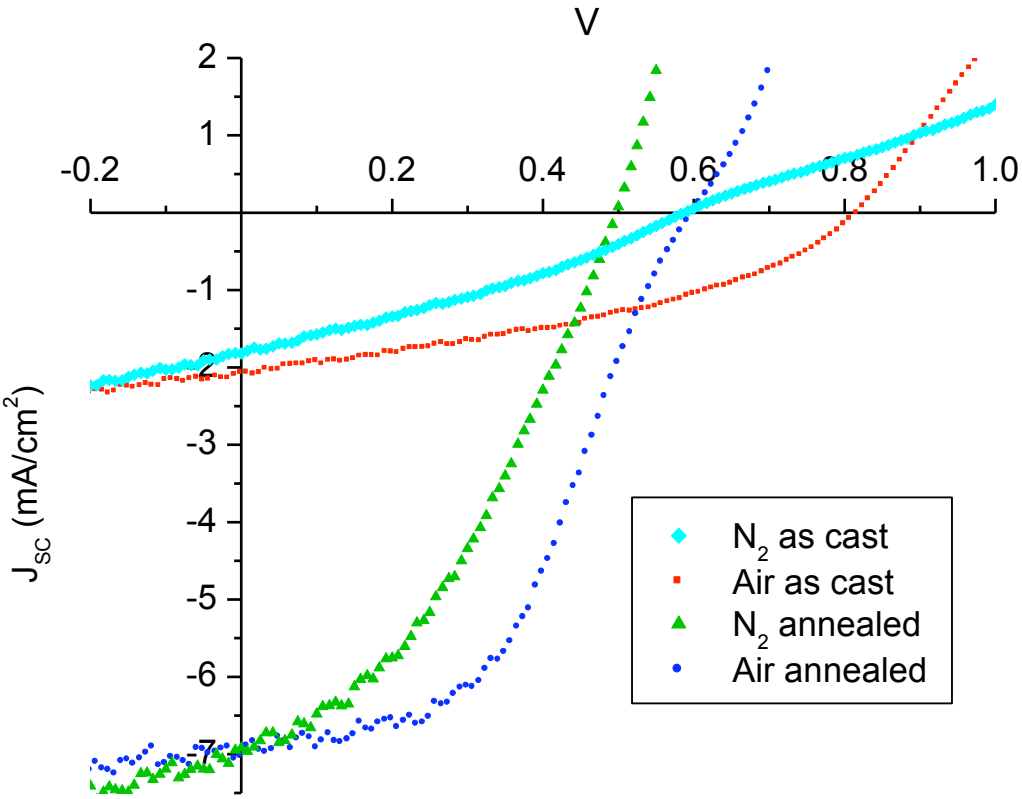

Figure 4.1. (color online) I-V curves of select cells from each set of exposure and annealing conditions. The curve for our highest-V_{OC} cell (0.82 V) is from the 1500 RPM set, the other three curves are from the 1200 RPM set.

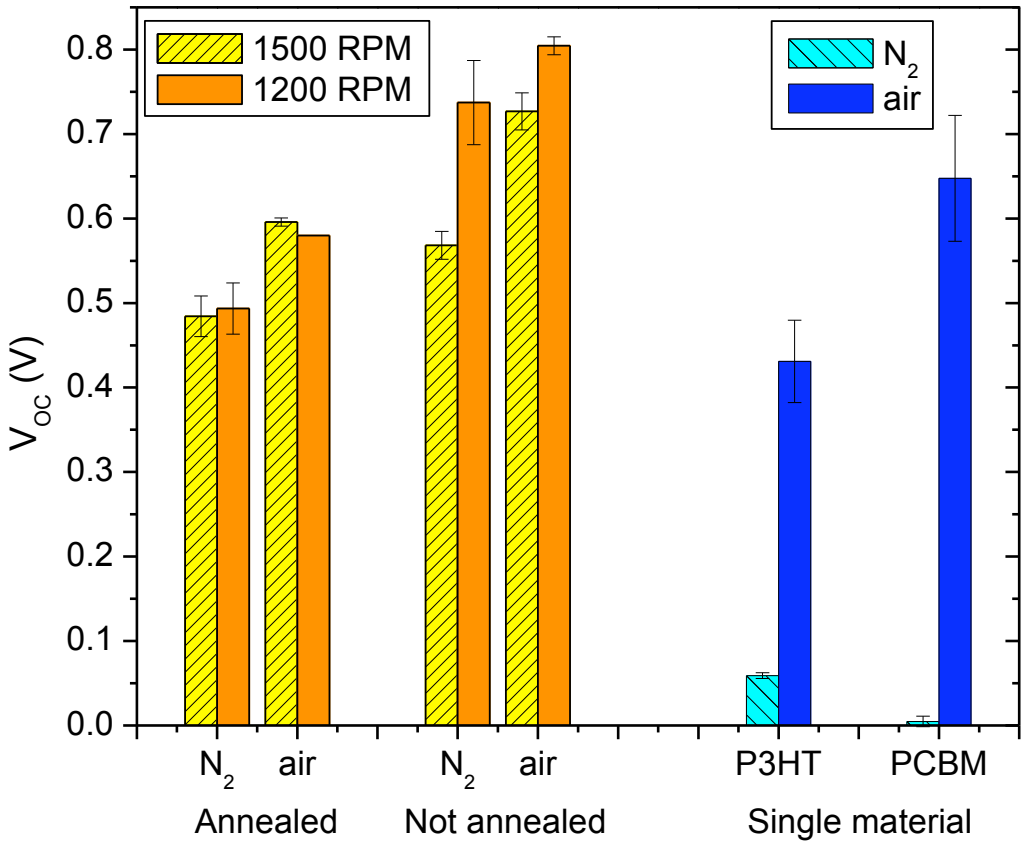

Figure 4.2 (color online) Open circuit voltage of various cells under 1 sun AM1.5G.

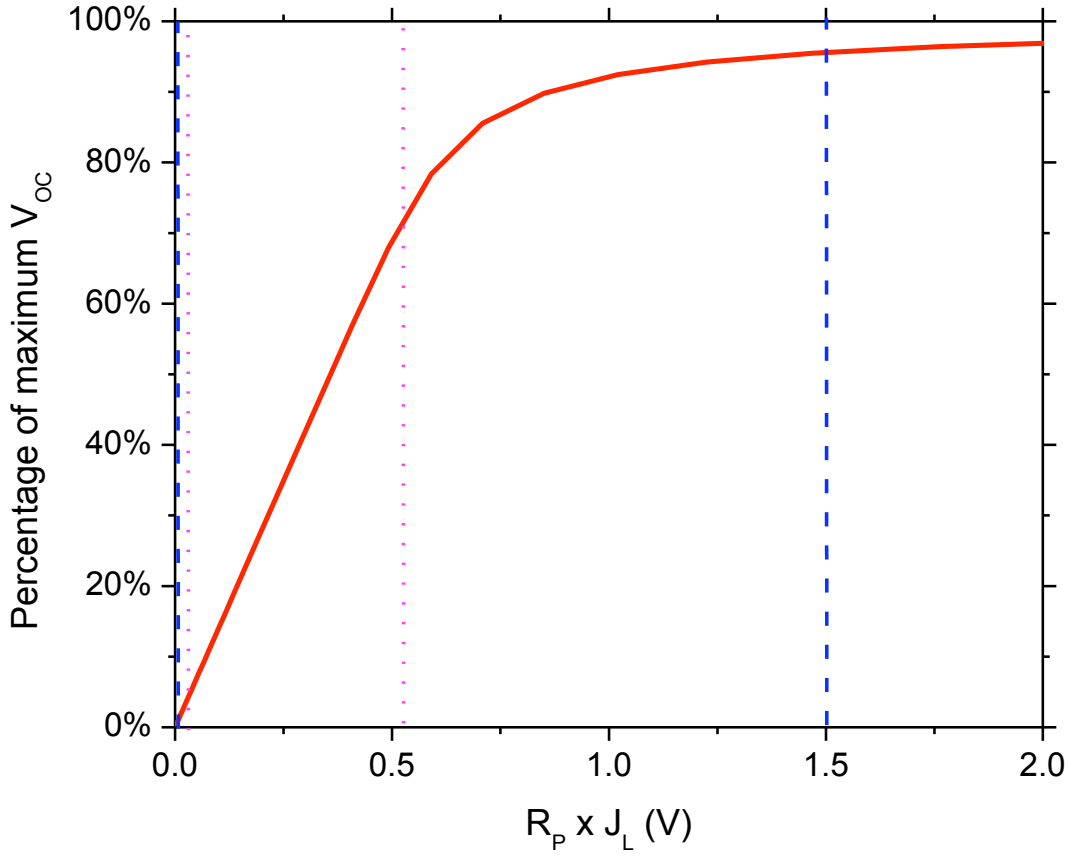

Figure 4.3 (color online) Percentage of maximum V_{OC} vs. R_P x J_L. Values used for calculating % of max V_{OC} were J_L = 1A and $J_0=10^{-6}$ A/cm^2. The trend does not hold for values of $J_0 \sim J_L$.

References

[1] D. Mühlbacher M. C. Scharber, M. Koppe, P. Denk, C. Waldauf, A. J. Heeger, C. J. Brabec,, "Design Rules for Donors in Bulk-Heterojunction Solar Cells - Towards 10 % Energy-Conversion Efficiency," Adv. Mater. **18** (6), 789-794 (2006).

[2] L. J. A. Koster, V. D. Mihailetchi, and P. W. M. Blom, "Ultimate efficiency of polymer/fullerene bulk heterojunction solar cells," Appl. Phys. Lett. **88** (9), 093511-093513 (2006).

[3] Maher Al-Ibrahim, H. Klaus Roth, Uladzimir Zhokhavets et al., "Flexible large area polymer solar cells based on poly(3-hexylthiophene)/fullerene," Sol Energ Mat Sol C **85** (1), 13-20 (2005).

[4] Michael D. Irwin, D. Bruce Buchholz, Alexander W. Hains et al., "p-Type semiconducting nickel oxide as an efficiency-enhancing anode interfacial layer in polymer bulk-heterojunction solar cells," Proceedings of the National Academy of Sciences **105** (8), 2783-2787 (2008).

[5] M. P. de Jong W. Osikowicz, W. R. Salaneck,, "Formation of the Interfacial Dipole at Organic-Organic Interfaces: C_{<FONT SIZE='-1'>60</FONT>}/Polymer Interfaces," Adv. Mater. **19** (23), 4213-4217 (2007).

[6] D. Cheyns, J. Poortmans, P. Heremans et al., "Analytical model for the open-circuit voltage and its associated resistance in organic planar heterojunction solar cells," Physical Review B (Condensed Matter and Materials Physics) **77** (16), 165332-165310 (2008).

[7] M. Kemerink, J. M. Kramer, H. H. P. Gommans et al., "Temperature-dependent built-in potential in organic semiconductor devices," Appl. Phys. Lett. **88** (19), 192108-192103 (2006).

[8] Barry P. Rand, Diana P. Burk, and Stephen R. Forrest, "Offset energies at organic semiconductor heterojunctions and their influence on the open-circuit voltage of thin-film solar cells," Physical Review B (Condensed Matter and Materials Physics) **75** (11), 115327-115311 (2007).

[9] M. Reyes-Reyes, K. Kim, and D. L. Carroll, "High-efficiency photovoltaic devices based on annealed poly(3-hexylthiophene) and 1-(3-methoxycarbonyl)-propyl-1-phenyl-(6,6)C-61 blends," Appl. Phys. Lett. **87** (8), 083506 (2005).

[10] Maher Al-Ibrahim, Oliver Ambacher, Steffi Sensfuss et al., "Effects of solvent and annealing on the improved performance of solar cells based on poly(3-hexylthiophene): Fullerene," Appl. Phys. Lett. **86** (20), 201120-201123 (2005).

[11] Gang Li, Vishal Shrotriya, Yan Yao et al., "Investigation of annealing effects and film thickness dependence of polymer solar cells based on poly(3-hexylthiophene)," J. Appl. Phys. **98** (4), 043704-043705 (2005).

[12] Youngkyoo Kim, Stelios A. Choulis, Jenny Nelson et al., "Device annealing effect in organic solar cells with blends of regioregular poly(3-hexylthiophene) and soluble fullerene," Appl. Phys. Lett. **86** (6), 063502-063503 (2005).

[13] Aurelien Du Pasquier, Steve Miller, and Manish Chhowalla, "On the use of Ga-In eutectic and halogen light source for testing P3HT-PCBM organic solar cells," Sol Energ Mat Sol C **90** (12), 1828-1839 (2006).

[14] BL Conover and MJ Escuti, "Laboratory Teaching Modules on Organic Electronics and Liquid Crystal Displays for Undergraduate and Graduate Education," Physics and Technology of Organic Semiconductor Devices **1115** (2009).

[15] M. Trenikhin, A. Bubnov, A. Nizovskii et al., "Chemical interaction of the In-Ga eutectic with Al and Al-base alloys," Inorganic Materials **42** (3), 256-260 (2006).

[16] G. Li V. Shrotriya, Y. Yao, T. Moriarty, K. Emery, Y. Yang,, "Accurate Measurement and Characterization of Organic Solar Cells," Adv Funct Mater **16** (15), 2016-2023 (2006).

[17] Christoph J. Brabec, Sean E. Shaheen, Christoph Winder et al., "Effect of LiF/metal electrodes on the performance of plastic solar cells," Appl. Phys. Lett. **80** (7), 1288-1290 (2002).

[18] Akinobu Hayakawa, Osamu Yoshikawa, Takuya Fujieda et al., "High performance polythiophene/fullerene bulk-heterojunction solar cell with a TiO[sub x] hole blocking layer," Appl. Phys. Lett. **90** (16), 163517-163513 (2007).

[19] S. H. Kim J. Y. Kim, H.-H. Lee, K. Lee, W. Ma, X. Gong, A. J. Heeger,, "New Architecture for High-Efficiency Polymer Photovoltaic Cells Using Solution-Based Titanium Oxide as an Optical Spacer," Adv. Mater. **18** (5), 572-576 (2006).

[20] Yun Zhao, Zhiyuan Xie, Yao Qu et al., "Effects of thermal annealing on polymer photovoltaic cells with buffer layers and in situ formation of interfacial layer for enhancing power conversion efficiency," Synthetic Met **158** (21-24), 908-911 (2008).

[21] Emily A. Weiss Ryan C. Chiechi, Michael D. Dickey, George M. Whitesides,, "Eutectic Gallium-Indium (EGaIn): A Moldable Liquid Metal for Electrical Characterization of Self-Assembled Monolayers13," Angewandte Chemie International Edition **47** (1), 142-144 (2008).

CONCLUSION AND OUTLOOK

The field of organic electronics still holds plenty of opportunity for exciting research. The interdisciplinary nature of the field includes chemistry, solid state physics, soft condensed matter, and a broad range of characterization techniques. Since few researchers are experts in all of these fields, much beneficial research has likely been overlooked. The following is an overview of further research which would be a natural extension of the work presented here.

Chapter 2 is somewhat tutorial in nature and does not easily lead to any further research besides what was mentioned in the chapter, namely using the change in absorption distribution vs. angle of incidence to study the relationship between IQE and the absorption profile, including using p-polarized light to observe effects of light absorption near the cathode.

Chapter 3 lays the foundation for a rigorous comparison between optical modeling and experimental testing of folded organic solar cells. It also introduces a general method which could be used by researchers who are developing novel materials to evaluate the potential of the folded structure for their materials.

Chapter 4 reveals the current lack of understanding of band alignment within organic solar cells which suggests much new research:

- The inclusion of PEDOT:PSS or other layers at the anode and dielectric layers at the cathode are well known to improve device performance. There is still some doubt about the nature of their role, however. Analyzing I-V data for devices with different structures should provide inside into their functions. Possible structure include active layers of P3HT, PCBM, P3HT/PCBM bilayers, and P3HT:PCBM BHJ, all with and without PEDOT:PSS or dielectric layers.

- Polaronic states exist within most of the common organic materials and affect band alignment via Fermi-level pinning at organic-organic and organic-metal interfaces. Measurements of HOMO and LUMO levels may in some cases actually be measuring the polaronic energy levels of the materials. This thinking could be applied to measurement methods to determine which states are in fact being measured, and possibly determine the correct HOMO, LUMO, and polaronic states.

- Bulk heterojunctions are a complicated mixture of two materials which partially phase separate on lengths scales from several to hundreds of nanometers, and often involve a gradient in material concentration and/or enrichment of one phase at the interfaces. How the bulk and surface composition and morphology relate to band alignment at the interfaces has not been investigated. Cyclic voltammetry (CV) and/or UPS could be used to probe the surface states and relate them to composition. Comparisons to device V_{OC} could also be made.

- Spontaneous charge transfer has been observed between P3HT and C_{60} (making similar charge transfer between P3HT and PCBM very likely) which shifts the relative vacuum levels of these materials by 0.6 V. Applying this shift to the current theory of the origin of the V_{OC} would increase the maximum V_{OC} to 1.4-2 V or more, which raises further questions as to where the voltage losses are occurring in organic devices. CV measurements of a bulk heterojunction of MEH-PPV:PCBM seemed to show a mixture of states from the two materials with an energy offset relative to each other. CV could then be used to detect interfacial band alignment. The alignment of PEDOT:PSS with different materials could also be tested by CV.